Geophys. J. R. astr. Soc. (1976) **46,** 605–646.

Glacial-Isostatic Adjustment—I. The Forward Problem

W. R. Peltier

Department of Physics, University of Toronto, Toronto, Ontario, Canada, M5S 1A7

and J. T. Andrews

Institute for Arctic and Alpine Research, University of Colorado, Boulder, Colorado 80302, USA

(Received 1976 February 27; in original form 1976 January 20)

Summary

The isostatic adjustment of a radially stratified visco-elastic spheroid is treated using space-time Green functions for the associated surface mass load boundary value problem. These impulse response functions are convolved with a Heaviside function to give the time dependent deformation of the planet which would be produced by a unit point mass brought up from infinity at $t = 0$ and allowed to remain on the surface. The resulting ' Heaviside Green functions ' can be employed to simulate all of the important signatures of glacial isostatic adjustment. Given a space-time dependent surface mass load consisting of ice sheet ablation histories and a model of the simultaneous filling of the ocean basins, these source terms are simply convolved with the Heaviside Green function appropriate to a specific response signature. A realistic model of the spatial distribution of the main late Pleistocene ice loads and of their temporal disintegration is constructed. The response of two visco-elastic earth models is computed and compared to a global set of relaxation data (relative sea-level curves). On the basis of this initial comparison of theory and observation the possibility that the lower mantle has a viscosity which is significantly in excess of the viscosity of the upper mantle is excluded. In addition, clear evidence of the presence of the lithosphere has been found in relaxation data from sites which were near the edge of the Laurentide ice sheet. Such data should therefore prove useful as a basis for analysis of lateral variations in lithosphere thickness. Further extensions of the calculation are suggested.

1. Introduction

Observations of the phenomenon of glacial isostatic adjustment provide an important constraint which any general theory of the rheology of the planetary interior must accommodate. The reason for the importance of this phenomenon derives from the time scale over which it occurs. This time scale, which is on the order of 10^3–10^4 yr, is ' intermediate ' between those time scales which separate the conventional realms of geological and geophysical concern. It is very much shorter than

that for mountain building or continental drift, yet very much longer than the period of a seismic body wave or elastic-gravitational free oscillation. In seeking to identify the forces which govern the adjustment process, it is not clear *a priori* whether these should be dominated by the forces which govern the short time-scale processes or those which are operative on geological time scales. For short time-scale processes the success of body wave and free oscillation seismology provides convincing evidence that the interior behaves essentially like a linear Hookean elastic solid subject to a gravitational body force. For long time-scale processes, we are on much less certain ground, but here the notion of an effective balance between gravitational forces and those which have a pseudo-viscous origin pervades the literature of the subject. As an example, the phenomenon of mantle convection is most often discussed subject to the assumption that on the time scale of continental drift the material behaves like a Newtonian viscous fluid (McKenzie, Roberts & Weiss 1974). Although it is possible to give plausibility arguments as to why this might be so, the subject is fraught with controversy, and the present fashion appears to be to attempt to work with non-Newtonian models.

Historically, the data of post glacial uplift have been rationalized by assuming a Newtonian constitutive relation for the interior (Haskell 1935, 1936, 1937; Vening Meinesz 1937; Niskanen 1948). This first approximation is easily understandable because the available data set is highly suggestive of a simple relaxation process. Modern observational data consists principally of relative sea level curves obtained by the C^{14} analysis of raised (submerged) beach material (Andrews 1974). McConnell (1963) was the first to attempt to invert relaxation data in the context of a linear visco-elastic model and to attempt simultaneously to deduce, via this inversion, a depth dependence for the viscosity of the mantle. However, his analyses were restricted to the consideration of plane earth geometries in the context of the Fennoscandian uplift, and it was never clear to what extent inclusion of the spherical topology of the real earth would alter the conclusions which he drew. In addition McConnell used a much reduced form for his linear viscoelastic constitutive relation which essentially amounted to the *a priori* neglect of the elastic response to unloading. His model was thus essentially a fluid model although more general than earlier versions in that it could accommodate an elastic lithosphere and variations of fluid viscosity with depth in the underlying asthenosphere. The viscosity model which he required to fit the Fennoscandia data had viscosity rapidly increasing as a function of depth (the increase over the first 2×10^3 km of the mantle was approximately 3 orders of magnitude). This notion that the viscosity of the mantle rapidly increases with depth was later supported by McKenzie (1966, 1967, 1968) who interpreted the so-called equatorial bulge of the Earth's figure as a fossil rotational bulge (Munk & MacDonald 1960) and was led to the same conclusion. Goldreich & Toomre (1969) showed that this idea was incorrect and deduced that the viscosity of the lower mantle should be in the range 10^{22}–10^{24} Poise in order to explain polar wandering (in the context of their own model of this phenomenon). O'Connell (1971) has supported this idea of a relatively low viscosity in the deep mantle by inverting the ancient eclipse data on the nontidal acceleration of the Earth's rotation in the manner suggested by Dicke (1966, 1969).

An important question therefore remains as to why the post glacial rebound data appear to require a high lower mantle viscosity. Brennan (1974) has recently attempted to reconcile the apparent dichotomy by suggesting that McConnell's result is an artifact of his assumption of a Newtonian viscosity. It is clear that this assumption is strictly correct only if the mechanism of mantle creep is governed by the diffusion of impurities (Herring–Naborro creep). The application of this creep mechanism to mantle processes was originally discussed by Gordon (1965, 1967). Weertman (1970) has recently shown that although diffusion creep may dominate if the strain rates are low enough, as the strain rates increase, the mechanisms of creep by dislocation

climb and dislocation glide eventually dominate. Both of these processes give rise to relations between stress and strain rate which are not linear and thus these processes are not Newtonian. Brennan has shown that if one assumes that the relation between stress and rate of strain is not Newtonian, then it is possible to reconcile McConnell's data on the rebound with a lower value for the deep mantle ' viscosity ' than the one which McConnell obtained.

There is, however, an alternative hypothesis which may allow such a reconciliation to be effected. This is simpler than the one advanced by Brennan, and it is that McConnell's result is an artifact of the plane topology in which he modelled the rebound process. Brennan's work suffers from the same basic inadequacy. We are led to consider this possibility for two reasons. Firstly Parsons' (1972) work on the viscosity inverse problem (again for plane geometry) has shown that the resolving power of the Fennoscandia data limits resolution to about the top 600 km of the mantle. McConnell's data were simply unsuitable for resolving viscosity structure much deeper than this. It is now possible to overcome this problem of lack of resolution at depth by using rebound data from the Laurentide ice sheet (Walcott 1972a, b) which covered a very much larger area than the one in Fennoscandia. Secondly, Cathles' (1971, 1975) work with the Laurentide data, which was the first to treat a detailed rebound problem in spherical geometry, suggests that no rapid increase of viscosity with depth may be necessary to accommodate the relative sea-level data and may even be prohibited by it.

The main purpose of the present paper is to reformulate the isostatic adjustment problem in spherical geometry and to provide a theory of this process which is sufficiently simple that it may be readily incorporated within the context of a rigorous inverse procedure for the determination of the depth dependence of mantle viscosity. If it is not possible to fit the relaxation data using this theory which is based upon the assumption of a linear visco-elastic constitutive relation, then of course the theory would have to be modified (perhaps to incorporate a non-Newtonian relation between stress and strain rate as Brennan has suggested). Even if it does prove possible to fit the data with this model, it may still be open to doubt.

The implication that the mantle behaves substantially *as if* it were a linear visco-elastic continuum over time scales as short as 10^3–10^4 yr would nevertheless be an important one in so far as the understanding of processes with longer time scales is concerned. If it can be established with reasonable certainty that the effective viscosity of the mantle is essentially uniform, then the hypothesis of mantle wide convection as a driving mechanism for continental drift becomes a much more tenable one. Peltier (1972) has shown that the radial mixing length for convection in such a system could well be on the order of the thickness of the mantle itself. This would make it possible to understand the large horizontal scales which are visible in the configuration of surface plates—an observation which is difficult to understand if one assumes that convection is confined to some surficial low viscosity channel. It has often been argued in the past that the rapid increase of viscosity with depth as *demanded* by the uplift observations was the physical mechanism whereby convection was confined to the uppermost layer of the system (McKenzie 1969). This confinement was *presumed* to be necessary in order to explain the confinement of seismicity within the top 650 km of the mantle. If the viscosity of the mantle is uniform and if convection must be confined to the upper mantle to explain the depth distribution of seismicity then a new mechanism for confinement must be sought. Perhaps such confinement may be effected by the phase change at 650 km depth but this possibility remains to be demonstrated.

The physical basis of the theory which we will employ in this reanalysis of the rebound observations is an extension of that given in Peltier (1974, hereafter referred to as Paper 1). In Section 2 this theory will be reviewed for the sake of completeness although the review will be a very cursory one. In Section 3 the basic computational

structure of the model will be presented, and in Section 4 the extensions of the original theory which are required by virtue of this computational structure will be given. In Section 5 the main computational difficulty with the extended theory is pointed out and a fairly simple method due to Farrell (1973) invoked for its solution. In Section 6 we describe a realistic model history of ice-sheet ablation in the Fennoscandia and Laurentide regions which is compatible with the new Quaternary geological data. This model is completely tabulated in the Appendix for the use of others who may wish to further pursue such calculations. In Section 7 we compare an approximate set of predicted relative sea level curves based upon two different visco-elastic earth models to actual observations. Our conclusions based upon this limited set of comparisons are listed in Section 8.

2. Impulse response Green functions

The cornerstone of the theory to be employed involves the construction of space-time Green functions for the basic surface mass load boundary value problem. This is a unique characteristic of our treatment of the adjustment process. As a constitutive relation for the material of the mantle, we employ a Maxwell relation between stress and strain so that on short time scales the material behaves like a Hookean elastic solid, while on long time scales it approaches asymptotically the behaviour of a Newtonian viscous fluid. A partial utilization of the Maxwell constitutive relation is illustrated by Cathles' (1971) work on the global problem. The treatment of the adjustment process given here differs from Cathles' work in several important respects which considerably extend the range of application of the theory and give it a simplicity which makes such application relatively straightforward. This simplicity is achieved through direct application of the Correspondence Principle (Malvern 1969) so that solutions are first obtained in the Laplace transform domain and then transformed to the time domain. Although these inversions are done approximately using an extremal technique, the accuracy obtained is easily sufficient for our purpose. The extension in the range of application is obtained through the construction of Green functions for the planetary model which simultaneously effects a pronounced increase in accuracy of the calculation. This increase in accuracy is, in fact, necessary for the modelling which is required. Since these Green functions can be constructed not only for radial displacement but also for gravity anomaly, tilt, and the perturbation in the ambient gravitational potential, it is simple to incorporate further observational constraints on the mantle viscosity profile beyond that provided by the relative sea level curves (i.e. present-day gravity anomalies due to incomplete compensation since deglaciation and data on the non-tidal acceleration of the Earth's rotation). Cathles' analysis, which was performed in the Legendre transform domain, obliged him to work in terms of truncated spherical harmonic expansions and to accept, without the possibility of easy control, the errors in representation which intrinsically limit such an approach.

The Maxwell constitutive relation is discussed in most basic books on continuum mechanics (e.g. Malvern 1969) and has the form

$$\dot{\tau}_{kl}+(\mu/\nu)\,(\tau_{kl}-\tfrac{1}{3}\tau_{kk}\,\delta_{kl}) = 2\mu\dot{e}_{kl}+\lambda\dot{e}_{kk}\,\delta_{kl} \tag{1}$$

where τ_{kl} and e_{kl} are respectively the stress and strain tensors; the dot denotes time differentiation; δ_{kl} is the unit diagonal tensor; μ and λ are the usual Lamé constants, and ν is the viscosity. To set up the problem for application of the Correspondence Principle we begin by subjecting (1) to Laplace transformation and thereby obtain

$$\left(s+(\mu/\nu)\right)\tilde{\tau}_{kl}-\tfrac{1}{3}(\mu/\nu)\,\tilde{\tau}_{kk}\,\delta_{kl} = 2\mu s\,\tilde{e}_{kl}+\lambda s\,\tilde{e}_{kk}\,\delta_{kl}, \tag{2}$$

where s is the Laplace transform variable (imaginary frequency). Contraction of the

tensor relation (2) gives

$$\tilde{\tau}_{kk} = (3\lambda+2\mu)\tilde{e}_{kk}. \tag{3}$$

Substitution of equation (3) back into equation (2) gives, in the usual fashion, the relation

$$\tilde{\tau}_{kl} = \left(\lambda+\tfrac{2}{3}\frac{(\mu/v)}{(s+\mu/v)}\right)\tilde{e}_{kk}\,\delta_{kl}+\frac{2\mu s}{(s+\mu/v)}\,\tilde{e}_{kl}. \tag{4}$$

Equation (4) can be written in the form

$$\tilde{\tau}_{kl} = \lambda(s)\,\tilde{e}_{kk}\,\delta_{kl}+2\mu(s)\,\tilde{e}_{kl} \tag{5}$$

where

$$\lambda(s) = \frac{\lambda s+\mu k/v}{s+\mu/v}, \qquad k = \lambda+\tfrac{2}{3}\mu, \qquad \mu(s) = \frac{\mu s}{s+\mu/v}. \tag{6}$$

Now equation (5) obviously has the same form as the constitutive relation for a Hookean elastic solid, where the corresponding Lamé parameters $\lambda(s)$ and $\mu(s)$ are now explicit functions of the Laplace transform variable s. According to the Correspondence Principle, we can construct the spectrum of the time dependent solution by solving the equivalent elastic problem for a range of values of the Laplace transform variable s using the constitutive relation (5). The problem of inverting the spectra constructed in this way, of course, remains. Cathles (1971, 1975), although he gave the standard development (1)–(6) of the Correspondence Principle, made no use of it in his analysis. This development plays a critical role in the theory presented here.

If we restrict ourselves to the consideration of small strains, then the Laplace transform domain form of the equations of motion, which consist of the linearized, equation of momentum conservation and Poisson's equation, are the following (Backus 1967) in which the inertial force is neglected because of the long time scale of the phenomenon under discussion:

$$\begin{aligned}\nabla.\tilde{\boldsymbol{\tau}}-\nabla(\rho g\tilde{\mathbf{u}}.\mathbf{e}_r)-\rho\nabla\tilde{\phi}+g\nabla.(\rho\tilde{\mathbf{u}})\mathbf{e}_r &= 0\\ \nabla^2\tilde{\phi} &= -4\pi G\nabla.(\rho\tilde{\mathbf{u}}).\end{aligned} \tag{7}$$

Here ρ and g are the density and gravitational acceleration in the hydrostatic equilibrium state, $\tilde{\mathbf{u}}$ is the displacement vector, $\tilde{\boldsymbol{\tau}}$ is the stress tensor, and $\tilde{\phi}$ is the gravitational potential perturbation; $\tilde{\phi}$ is the sum of the two parts, $\tilde{\phi}_1$ and $\tilde{\phi}_2$, which are respectively, the perturbation potential of the ambient gravitational field and the potential of the externally applied gravitational force field (the load). $\mathbf{e}_r$ is a unit vector in the radial direction. The tilde indicates implicit dependence upon the Laplace transform variable s which enters (7) through $\tilde{\boldsymbol{\tau}}$ defined in (5). We elect to restrict our attention to spherically symmetric earth models with a free outer surface (except at the point of application of a load) and look for Laplace transform domain solutions for the deformation due to a point mass. Under these restrictions (7) reduces to the spheroidal system of equations in the three variables $\tilde{u}_r$, $\tilde{u}_\theta$, and $\tilde{\phi}$. When $\tilde{\mathbf{u}}$ and $\tilde{\phi}$ are expanded in vector spherical harmonics and explicit use is made of the symmetry of the problem, then (dropping the tilde)

$$\left.\begin{aligned}\mathbf{u} &= \sum_{n=0}^{\infty}\left(U_n(r,s)\,P_n(\cos\theta)\mathbf{e}_r+V_n(r,s)\frac{\partial}{\partial\theta}P_n(\cos\theta)\mathbf{e}_\theta\right)\\ \phi &= \sum_{n=0}^{\infty}\phi_n(r,s)\,P_n(\cos\theta).\end{aligned}\right\} \tag{8}$$

We introduce three additional dependent variables as the radial and tangential components of the stress tensor τ_{rr} and $\tau_{r\theta}$ respectively and a functional q related to the

radial gradient of potential and thus to the ambient gravitational field as

$$q = \frac{\partial \phi}{\partial r} + \frac{(n+1)}{\Gamma}\phi + 4\pi G\rho u_r. \tag{9}$$

By also expressing these variables in terms of their Legendre transforms with coefficients $T_{r,n}$, $T_{\theta,n}$ and Q_n, equations (7) reduce to the matrix equation

$$\frac{d\mathbf{Y}}{dr} = \mathbf{A}\mathbf{Y} \tag{10}$$

where $\mathbf{Y} = (U_n, V_n, T_{r,n}, T_{\theta,n}, \Phi_n, Q_n)$ and $\mathbf{A}$ is the s dependent matrix given in Paper 1. The boundary conditions required for the solution of (10) and other details of this phase of the calculation are also discussed in Paper 1. The problem is analogous to the elastic problem of ocean tidal loading which has been treated by Farrell (1973), using a similar approach to the one adopted here.

In analogy with this problem we proceed to define a set of dimensionless Love numbers h_n, k_n, and l_n which are functions of the three variables r, n and s. If U_n, V_n, and $\Phi_{1,n}$ arise from a field of force with potential ϕ_2 and coefficients $\Phi_{2,n}$, these Love numbers are defined as

$$\begin{bmatrix} U_n(r,s) \\ V_n(r,s) \\ \phi_{1,n}(r,s) \end{bmatrix} = \Phi_{2,n}(r) \begin{bmatrix} h_n(r,s)/g \\ l_n(r,s)/g \\ k_n(r,s) \end{bmatrix}. \tag{11}$$

The function $\Phi_{2,n}$ in (11) is independent of s since the applied load is assumed to have a delta function dependence in the time domain. If $\Phi_{2,n}$ derives from a point mass on the surface then the solution of (10) gives the impulse response of the linear system.

In Paper 1 we discussed the relaxation characteristics of three different visco-elastic models, the elastic properties of which (their radially dependent Lamé parameters) were all taken to be those of the Gutenberg–Bullen model A earth (Alterman, Jarosch & Pekeris 1961). These models have viscosity structures as shown in Fig. 1 (Models 1, 2 and 3) and their characteristics will be further developed in the context of the present discussion. These models are similar to some discussed by Cathles (1971) although not identical.

The Love number s-spectra for model 1 as deduced by multiple integrations of the set of simultaneous ordinary differential equations (10) are shown in Fig. 2 of Peltier (1976) (companion paper, hereafter Paper 2) for h_n where r is taken equal to the Earth's radius. The l_n spectra are not required in the present analysis. The most apparent characteristic of these spectra is the existence of the asymptotic regimes for large and small values of s. These asymptotic regimes correspond respectively to the elastic and isostatic limits as discussed in Papers 1 and 2. The inversion of these spectra is facilitated by splitting off the constant large s asymptote as

$$\left.\begin{aligned} h_n(s) &= h_n^V(s) + h_n^E \\ k_n(s) &= k_n^V(s) + k_n^E. \end{aligned}\right\} \tag{12}$$

We may then formally express the Laplace inversion of (12) as

$$\left.\begin{aligned} h_n(t) &= L^{-1}[h_n^V(s)] + h_n^E\delta(t) \\ k_n(t) &= L^{-1}[k_n^V(s)] + k_n^E\delta(t). \end{aligned}\right\} \tag{13}$$

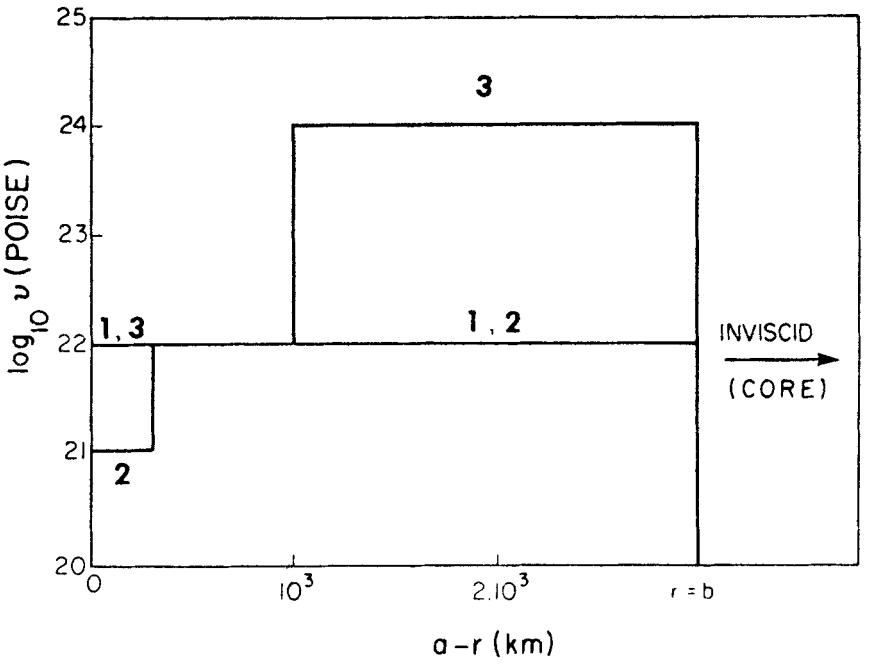

FIG. 1. Radial viscosity profiles for Models 1–3.

The weights h_n^E and k_n^E are then just the surface mass load Love numbers which have been calculated by previous authors for the elastic problem (Kaula 1963; Kuo 1969; Farrell 1972). Inversion of the anelastic parts of the Love number s-spectra is discussed in Paper 1 and leads to approximate expressions for the time histories in the form of Dirichlet series. If $\theta(s)$ is any one of $h_n^V(s)$ or $k_n^V(s)$, we find

$$\theta(t) = \sum_{i=1}^{m} r_i \exp(-t/\tau_i) \tag{14}$$

where the r_i may be thought of as a discrete approximation to the characteristic distribution function of relaxation times τ_i for each harmonic n and for either the h or k Love number. See Paper 2 for a discussion of the relation between this approximate solution and the exact solution. The anelastic parts of the Love number time histories are illustrated by the $h_n^V(t)$ of Model 1 in Fig. 5 of Paper 2 for a series of harmonics. This plot is Log-Linear so that deviation of the time history on the plot from a straight line indicates a highly non-exponential mode of decay. The reasons for such non-exponential behaviour are thoroughly discussed in Papers 1 and 2.

We proceed to construct impulse response Green's functions by summing series of the form (8). The expression for radial displacement, for example, can be reduced to the following form using (11)

$$u_r(\theta, t) = \frac{a}{m_e} \sum_{n=0}^{\infty} [h_n^V(t) + h_n^E \delta(t)] P_n(\cos\theta) \tag{15}$$

The summation of such infinite series is discussed in Paper 1 where similar expressions for the gravity anomaly and tilt are also obtained following the work of Longman

(1963) and Farrell (1972). The elastic part of the Green function for radial displacement (that with the $\delta(t)$ time dependence) was partially computed by Longman (1963) and completely by Farrell (1972). The viscous part was obtained in Paper 1 and is illustrated for Model 1 in Fig. 8 of Paper 2 (see Paper 1 for the analogous functions for gravity anomaly and tilt). Perhaps the most important aspect of these Green functions is the obvious presence of the peripheral bulge and the manner in which this bulge migrates inwards after load removal. This aspect of the response has obvious implications concerning lower mantle viscosity as discussed in Paper 1.

In the next section we proceed to discuss the way in which the Green functions described above may be employed in a detailed discussion of the isostatic adjustment process.

3. Modelling the adjustment process

Application of the Green functions developed in Paper 1 to the simulation of isostatic adjustment requires some extension of the formalism. Suppose that at some time $t = 0$ in the past the Earth was in a state of isostatic equilibrium and that its shape was perfectly spherical. We choose to associate this time with the maximum in the Wisconsin glaciation at approximately 18 KYBP (18 000 BP). At that time the glacial ice began to melt, and the resulting meltwater was added as a load to the ocean basins. This redistribution of mass upsets the gravitational equilibrium characteristic of the state of isostatic equilibrium and the system consisting of planet plus ice plus water tends towards a new configuration in which the total mass of the system is again in gravitational equilibrium. This is the process of isostatic adjustment which we are to model. It is a process which clearly demands a redistribution of mass in the planetary interior. Part of this redistribution of mass is effected elastically; and since the problem is treated quasi-statically, this elastic adjustment occurs instantaneously with every shift in surface load. The remainder of the required mass redistribution is accomplished anelastically, and this anelastic compensation proceeds via mass transport in the interior. The unbalanced gravitational force sets up a transient convection to accomplish this purpose.

Here we will concentrate for definiteness upon describing the adjustment process in terms of the change in shape of the planet. This change in shape will be known as a function of time once we specify the time dependence of the radius of each location on the initially spherical surface. This will suffice since we are treating a phenomenon involving small strains so that the final shape of the planet will also be nearly spherical. This assumption of small strain can be justified *a posteriori*. The time histories of local radius are intimately connected with the relative sea level curves which form the most important observational datum of the process. More exactly these observational data describe the time dependent separation between two potential surfaces which may be calculated exactly as described in a second companion paper (Farrell & Clark 1976).

Let us suppose initially that we are to remove a load $L(\theta, \lambda)$ instantaneously from the surface of the planet at $t = 0$ where the variables θ and λ are respectively the co-latitude and east-longitude (measured with respect to Greenwich) of points on the spherical surface. This load has units of kilograms. The time dependence of the change in radius at the surface point with co-ordinates (θ, λ) is simply obtained by convolving the radial displacement Green function with the surface load as

$$\Delta R(\theta, \lambda, t) = \int\int d\Omega' \int_0^t dt'\, G_R(\theta-\theta', \lambda-\lambda', t-t')\, H(t')\, L(\theta', \lambda') \tag{16}$$

where $d\Omega'$ is an element of surface area, G_R is the radial displacement Green function

and the Heaviside step function $H(t')$ appears in the integrand because we are assuming that the load $L(\theta, \lambda)$ is removed instantaneously. Now the Green function G_R depends only upon the source point-field point separation which we can express through an angle γ and is given by (15) or with γ written explicitly

$$G_R(\gamma, t) = \frac{a}{m_e} \sum_{n=0}^{\infty} h_n(t)\, P_n(\cos\gamma), \tag{17}$$

where $h_n^V(t)$ and $h_n^E \delta(t)$ have been lumped together. Thus

$$G_R\,(\gamma, t-t') = \frac{a}{m_e} \sum_{n=0}^{\infty} h_n\,(t-t')\, P_n\,(\cos\gamma) \tag{18}$$

and substitution of this expression into (16) gives the form

$$\Delta R(\theta, \lambda, t) = \int\int d\Omega'\, L(\theta', \lambda') \frac{a}{m_e} \sum_{n=0}^{\infty} P_n(\cos\gamma) \int_0^t dt'\, h_n(t-t')\, H(t'). \tag{19}$$

However, the convolution in time which is the inner integral in (19) may be done analytically on account of the Dirichlet series approximation which we have adopted for the Love number time histories in equation (14). In fact, the exact solutions described in Paper 2 have the same property. From (14) we then have

$$h_n(t-t') = \sum_{j=1}^{m} r_j \exp\!\left(-(t-t')/\tau_j\right) + h_n^E \delta(t-t'). \tag{20}$$

The temporal convolution in (19) thus becomes

$$\int_0^t dt'\, h_n(t-t')\, H(t') = \sum_{j=1}^{m} r_j\, \tau_j \left(1-\exp(-t/\tau_j)\right) + h_n^E. \tag{21}$$

We next define a set of Heaviside Love number time histories as

$$h_n^{H,V}(t) = \sum_{j=1}^{m} r_j\, \tau_j \left(1-\exp(-t/\tau_j)\right) \tag{22}$$

for the anelastic part thus reducing (19) to the form

$$\Delta R(\theta, \lambda, t) = \int\int d\Omega'\, L(\theta', \lambda') \frac{a}{m_e} \sum_{n=0}^{\infty} P_n(\cos\gamma)\, [h_n^{H,V}(t) + h_n^E]. \tag{23}$$

A set of Heaviside Love number time histories is shown in Fig. 2 for model 1 and $h_n^{H,V}(t)$ defined in equation (22). Each of these Love numbers saturates after a certain time which clearly depends upon the particular viscosity model of the interior as well as upon the degree of the Love number. Once the long time asymptote has been obtained the particular Love number, is isostatically adjusted.

The point of the above exercise is that we can now define a Heaviside Green function which we denote by $G_R^H(\gamma, t)$ as the sum of two parts as before such that

$$G_R^H(\gamma, t) = G_R^E(\gamma) + G_R^{H,V}(\gamma, t) \tag{24}$$

but now the temporal part of the original three variable convolution has been done analytically. Instead of constructing Green functions for the impulse response of the system as described in the previous section, we construct the Heaviside Green function

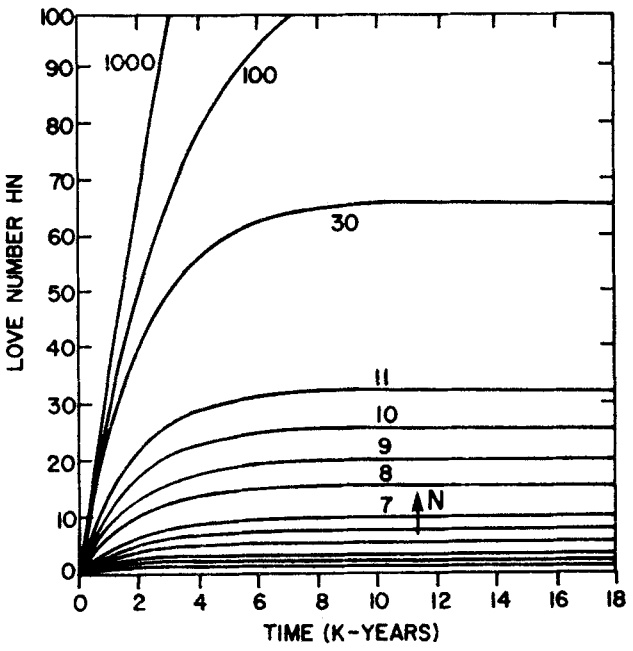

FIG. 2. Heaviside Love number time histories for $h_n^{H,V}$ for viscosity Model 1. The corresponding values of n are shown adjacent to each curve.

$G_R^{H,V}(\gamma, t)$ for the anelastic part by using the anelastic Heaviside Love number time histories in (22). Equation (23) then becomes simply

$$\Delta R(\theta, \lambda, t) = \int\int d\Omega' \, L(\theta', \lambda') \, [G_R^{E}(\gamma) + G_R^{H,V}(\gamma, t)] \tag{25}$$

and to evaluate the change in radius at any particular time after removal of the load only a single two variable convolution in the space domain is required. (Of course, the elastic part of the Green function is included in the convolution only at $t = 0$ where $G_R^{H,V}(\gamma, 0) = 0$.) The structure of these Heaviside Green functions will be described in the next section.

In general, the history of load removal or addition at each point in space does not take place in a single stage but rather consists of a continuous variation. We may approximate this continuous variation by a series of discrete variations and write

$$L(\theta, \lambda, t) = \sum_{i=1}^{N} L_i(\theta, \lambda) \, H(t - t_i). \tag{26}$$

We assume for simplicity that each of these discrete variations takes place in concert at each point in space.

At each stage in the load removal history we must ensure that the net mass added to the system is identically zero. Thus, over some region of the surface from which ice is being removed the function $L(\theta, \lambda)$ will be negative, and over some other part of the system (the ocean basins) the function $L(\theta, \lambda)$ will be positive. At each of the N stages of the process described by (26) the integral of $L(\theta, \lambda)$ over the surface must vanish in order to conserve mass.

A further problem which arises at this stage concerns the manner in which the meltwater is added to the ocean basins (the positive part of the load). It is conventional to assume that the meltwater is added to the oceans at each stage as a uniform sheet. This is strictly speaking impossible since such an addition of mass would produce an ocean whose surface is not an equipotential surface and which would thus not be in equilibrium. The idea that the meltwater raises the level of the ocean uniformly everywhere is the basis of the concept of eustatic (absolute) sea level. By looking at the ages of submerged marine deposits (shells, etc.) in a region which is assumed to be stable geologically, one can estimate the rise in eustatic sea level and knowing the area of the ocean basins calculate the rate and amount of mass loss from the glaciated regions (Shepard & Curry 1967). Bloom (1967) and Walcott (1972a) have pointed out an error in this assumption. This error, however, is due both to the invalid assumption of uniform mass addition to the oceans and to the assumption that the ocean basins are not involved in the adjustment process. On the basis of the discussion above, part of the ocean basin adjustment must be elastic and part pseudoviscous.

Farrell (1973) has given a method whereby the correct ocean basin filling model can be constructed taking into account the constraint that the ocean surface must remain an equipotential. He employed it to compute the effect of elastic yielding upon the oceans' tides. This method requires the Green function for the gravitational potential perturbation which was not determined in the calculations presented in Paper 1. The Heaviside form of the Green function will, however, be given in the next section. With this Green function it is possible to construct a consistent model for the filling of the ocean basins and to correctly determine the space and time dependent rise of sea level, and thus the time dependent bathymetry of the ocean basins. The structure of the theory required for this calculation is thoroughly described in a companion paper (Farrell & Clark 1976).

The calculation of signatures of the isostatic adjustment process is thus connected with the evaluation of two variable convolution integrals of the form (25). Since one such convolution must be performed for each point in time that the response is desired, some fast method for their evaluation is obviously necessary. Such a method (due to Farrell 1973) is discussed in Section 5. In the next section we describe the Heaviside Green functions for radial displacement, gravity anomaly, tilt, and gravitational potential perturbation which are required in the present theory.

4. Heaviside Green functions

The solution of the adjustment problem embodied in equation (25) requires for its implementation the calculation of Heaviside Green functions as defined in the last section. This calculation again involves the summation of infinite series of the type (15) with the $h_n^V(t)$ and $k_n^V(t)$ replaced in these summations by their Heaviside equivalents. $h_n^V(t)$, for example, is simply replaced by the $h_n^{H,V}(t)$ given in equation (22) and illustrated for one viscosity model by Fig. 2. All of the techniques described in Paper 1 for speeding convergence of the resulting series are again application, and no further numerical tricks are required. The mathematical forms of these Green functions are given in equations (27)–(30) inclusive for radial displacement, gravity anomaly, surface tilt, and gravitational potential perturbation, respectively.

$$h_n^H(\theta, t) = \frac{a}{m_e} \sum_{n=0}^{\infty} [h_n^{H,V}(t) + h_n^E] P_n(\cos\theta) \tag{27}$$

$$g^H(\theta, t) = \frac{g}{m_e} \sum_{n=0}^{\infty} \{n + 2[h_n^{H,V}(t) + h_n^E] - (n+1)[k_n^{H,V}(t) + k_n^E]\} P_n(\cos\theta) \tag{28}$$

$$t^H(\theta, t) = \frac{-1}{m_e} \sum_{n=0}^{\infty} \{1 - [h_n^{H,V}(t) + h_n^E] + [k_n^{H,V}(t) + k_n^E]\} \frac{\partial P_n(\cos\theta)}{\partial\theta} \tag{29}$$

$$\phi^H(\theta, t) = \frac{ag}{m_e} \sum_{n=0}^{\infty} \{1 - [h_n^{H,V}(t) + h_n^E] + [k_n^{H,V}(t) + k_n^E]\} P_n(\cos\theta). \tag{30}$$

Heaviside Green functions for Model 1 are shown in Figs 3–6 inclusive, respectively for radial displacement, gravity anomaly, tilt and gravitational potential perturbation. These Green functions have been normalized by the factors given, all of which serve to remove the effect of the singularity at the source point $\theta = 0$. All of the Green functions should thus approach an asymptote as $\theta \to 0$, and on most of the graphs shown this is indeed the case. We will return to a discussion of the nature of this small θ asymptote momentarily.

Inspection of Fig. 3 which shows the Heaviside Green function for radial displacement in Model 1 continues to reveal the presence of the peripheral bulge although perhaps not so clearly as was evident in the corresponding impulse response Green function discussed previously in Paper 1. This is not surprising since the impulse response Green function describes free decay whereas the Heaviside form describes the time evolution of a forced deformation. As $t \to \infty$, the peripheral bulge grows from essentially zero at $t = 0$ (its elastic expression) to some final amplitude which by inspection of Fig. 3 is virtually established after $t = 18\,000$ yr, the maximum time over which the Green function has been evaluated. For this viscosity model the bulge

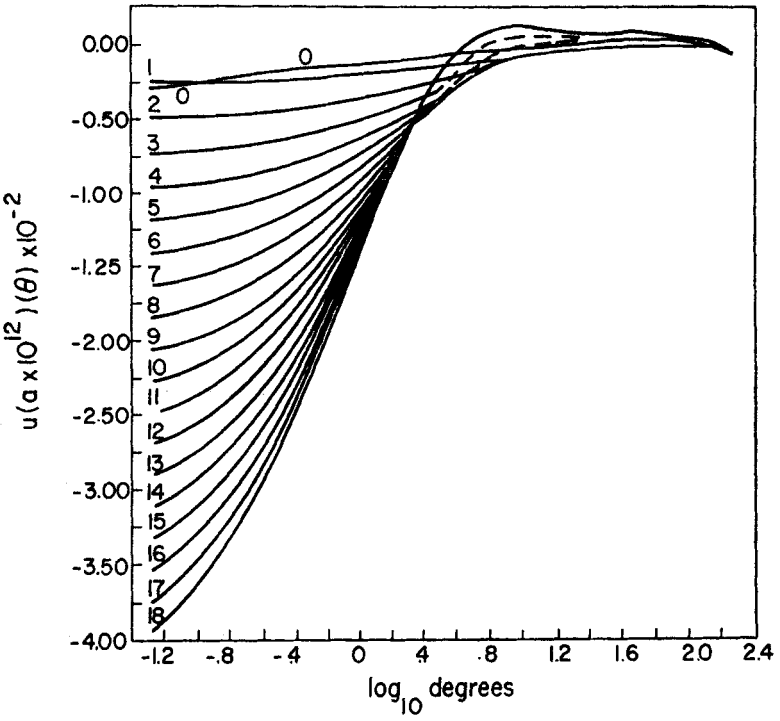

FIG. 3. Viscous part of the Heaviside Green function for radial displacement in Model 1. Normalization factor marks on the abscissa removes the r^{-1} singularity at $\theta = 0$. Times adjacent to each curve are in thousands of years after application of the load. $t = 0$ is the elastic Green function.

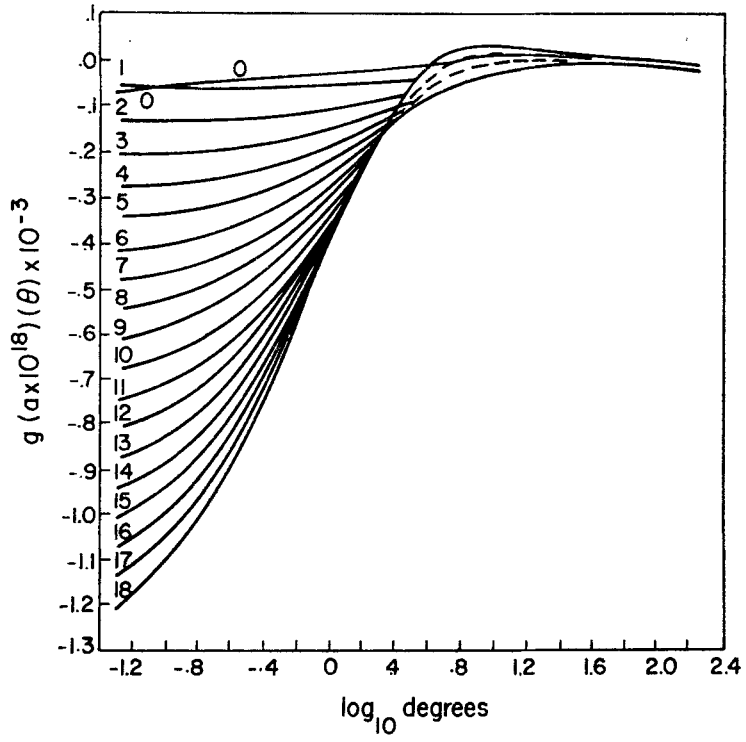

FIG. 4. Viscous part of the Heaviside Green function for gravity anomaly. Otherwise as in Fig. 3.

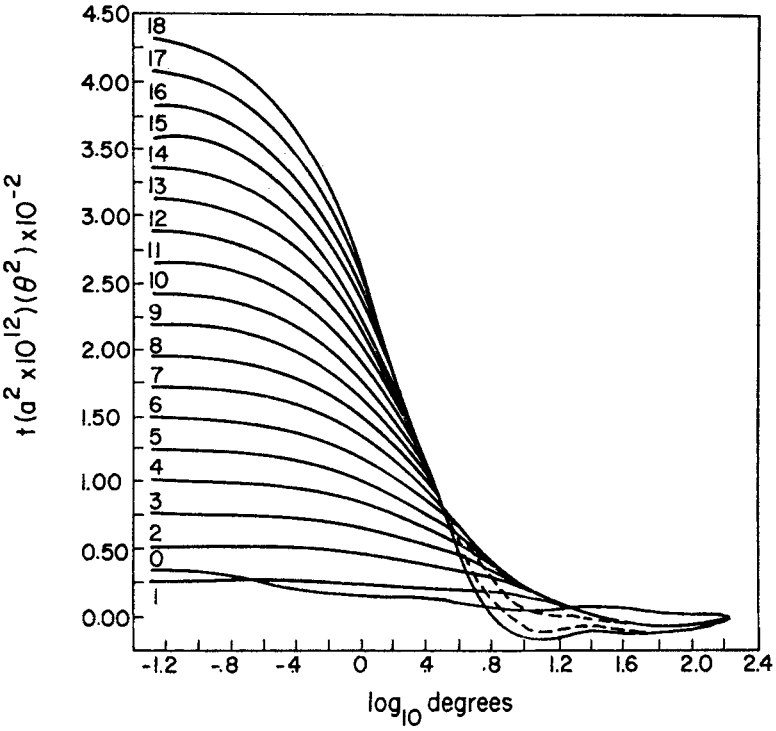

FIG. 5. Viscous part of the Heaviside Green function for tilt. Otherwise as in Fig. 3.

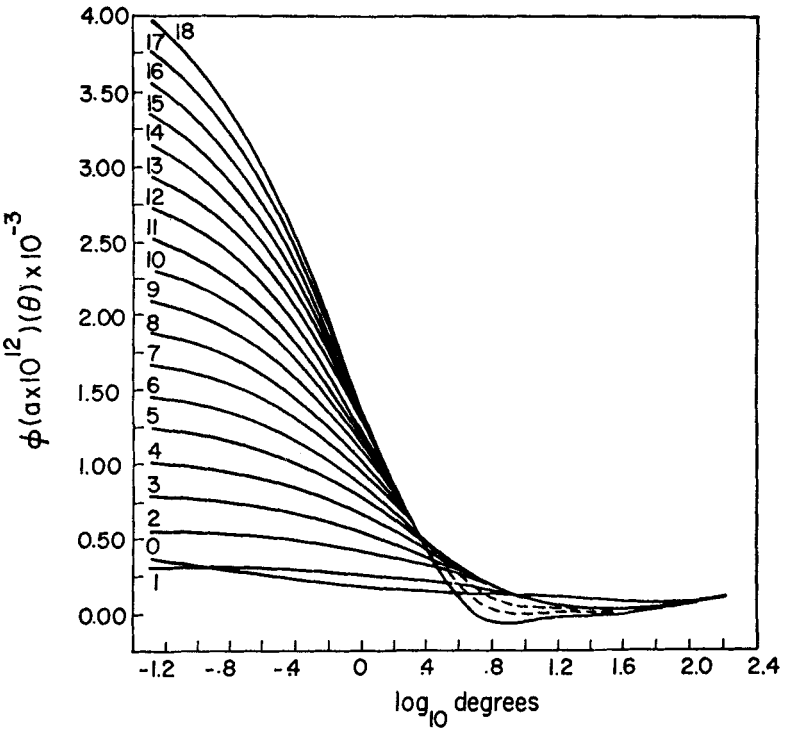

FIG. 6. Viscous part of the Heaviside Green function for gravitational potential perturbation. Otherwise as in Fig. 3.

is thus in isostatic equilibrium after a time on this order. Further information is very difficult to extract visually from the response functions alone. The Green functions for viscosity Models 2 and 3 will not be shown here since they are at least visually similar to those for Model 1. The Green functions for Model 1 have been tabulated for 1000-yr intervals and will be made available upon request.

Perhaps the main feature of mathematical interest in these functions is the uniformity of the time dependence of the strength of the singularity at $\theta = 0$. Inspection of any one of the Green functions shown above which are calculated at equi-spaced time intervals of 10^3 yr shows that the strength of the singularity is a linear function of the time after load application. Since the correct calculation of the strength of this singularity is critical to the convolution procedure which will be described in the next section, it is worthwhile at this point to go through the exercise of demonstrating why this particular time dependence should be obtained. The key to understanding this point is the recognition that for sufficiently small θ the response of the sphere should become asymptotically equivalent to the response of a homogeneous half space with bulk properties equal to those in the topmost layer of the radially stratified sphere. Here, of course, we are dealing with a visco-elastic material and so the particular half-space solution which is required is the visco-elastic analogue of the classical Boussinesq problem in static elasticity. We give a discussion of the solution to the problem of the time dependence of the singularity at $\theta = 0$.

Neglecting inertial forces, the Laplace transform displacement vector $\tilde{\mathbf{u}}$ is a solution of the equivalent elastic equilibrium equation everywhere in the half space. This equation has the form

$$\sigma(s)\,\nabla(\nabla.\tilde{u}) - \mu(s)\nabla\times\nabla\times\tilde{u} = 0 \tag{31}$$

where $\lambda(s)$ and $\mu(s)$ are the equivalent Lamé parameters defined in (6) and where $\sigma(s) = \lambda(s)+2\mu(s)$ and $\eta(s) = \lambda(s)+\mu(s)$. We solve (31) in the region $z \leqslant 0$ with the boundary condition that the surface $z = 0$ is stress free everywhere except at the origin where it is subject to a point force. If we assume that the point force has a delta function dependence in the time domain, then in the Laplace transform domain where (31) is valid the spectrum of the point force is constant. In Paper 1 equation (31) was solved for the vertical displacement $\tilde{u}(0, r)$ on the surface $z = 0$ as a function of s. This solution was found as

$$\tilde{u}(0, r) = -\frac{1}{4\pi r}\frac{\sigma(s)}{\mu(s).\eta(s)} = \left[-\frac{1}{4\pi r}\right]\left[\frac{s+\mu/v}{\mu s} + \frac{s+\mu/v}{(\lambda+\mu)s+\mu k/v}\right]. \tag{32}$$

This simple algebraic s-spectrum can be inverted analytically to give the exact time dependent solution $u(0, r)$ as

$$u(0, r) = \int_L \tilde{u}(0, r)\exp(st)\,ds \tag{33}$$

where L in (33) is the usual Bromwich path. Thus

$$u(0, r) = \left[-\frac{1}{4\pi r}\right]\left[\frac{\sigma}{\mu\eta}\delta(t) + \frac{1}{v} + c\exp(-t/\tau)\right] \tag{34}$$

where

$$\left.\begin{aligned} c &= \frac{\mu}{\eta v}\left[1-\frac{k}{\eta}\right] \\ \tau &= \frac{v\eta}{\mu k}. \end{aligned}\right\} \tag{35}$$

To obtain the Heaviside Green function for vertical displacement from the impulse response form (34) we simply convolve as usual with a Heaviside step function and in this way obtain

$$u^H(0, r) = \left[-\frac{1}{4\pi r}\right]\left[\frac{\sigma}{\mu\eta} + \frac{t}{v} + c\tau(1-\exp(-t/\tau))\right]. \tag{36}$$

The meaning of each of the three terms in (36) is exactly analogous to corresponding terms in the solution of the full spherical problem. The first term is the elastic component of the Green function first deduced by Boussinesq. The third term is completely analogous to the Heaviside Love number time histories defined in equation (22) for the spherical problem.

The second term in (36) is the one which eventually determines the time dependence of the r^{-1} singularity. After sufficiently long time ($t \gg \tau$), the third term becomes equal to a constant while the second continues to increase linearly. For the visco-elastic parameters of Models 1–3 the critical time for dominance of the second term is on the order of a few hundred years so that the amplitude of the singularity should increase linearly with time over virtually the entire loading history. As mentioned previously, this linear increase of the strength of the singularity with time is exactly what is observed in the spherical Heaviside Green functions as shown in Figs. 3–6.

In the above analysis, which was based upon the analogy with Boussinesq's problem, the medium was taken to be non-gravitating, since in this equivalent elastic problem use of conventional values for λ, μ, ρ and the deformation wavelength shows that elastic forces dominate the gravitational forces. If we carry this approximation

over to the viscoelastic problem, as we have done in the above discussion, then the gravitational potential perturbation in the visco-elastic Boussinesq problem may be found approximately by neglecting the elastic gravitational coupling and solving Poisson's equation

$$\nabla^2\phi = -4\pi G\rho\nabla.\tilde{\mathbf{u}} \tag{37}$$

using for components of $\tilde{\mathbf{u}}$ those determined in the previous analysis. The normal component of this $\tilde{\mathbf{u}}$ is given explicitly in (32). Following this method of analysis demonstrates that both the gravitational potential perturbation ϕ and the gravity anomaly g have a time dependence whose amplitude is ultimately linear which is again in accord with the observed behaviour of the Heaviside Green functions discussed above.

5. Convolution on the sphere

The numerical problem which we have to face in the course of implementing the global theory of isostatic adjustment formulated in the preceding sections is connected with the calculation of the two-dimensional convolution integrals of the form given in equation (25). The technique which we employ here is one described by Farrell (1973) in his treatment of the elastic ocean tidal loading problem. In the present context the need for a fast computational algorithm is readily apparent since we are obliged to calculate one full spherical convolution for each stage in the adjustment process in which we are interested. Of course, we need a sufficient number of time points in the relaxation histories to resolve all significant details of the process. We elect initially to sample the relaxation curves at 10^3-yr intervals which is just the spacing between time slices through the Green functions shown in Figs 3–6. This choice of temporal resolution may be adjusted later as we accrue experience in doing such calculations, but for the present such resolution would appear more than adequate given the resolution of the relative sea level data which we shall be obliged to fit (Andrews 1969; Walcott 1972a).

In doing convolutions of the form (25) we shall have to impose some degree of spatial resolution on the calculation, as well as the temporal resolution discussed above. Again we shall adopt a spatial resolution for these calculations which is compatible with the extent of our knowledge of the space dependence of the physical processes involved. Such knowledge is at present almost entirely confined to information on the spatial extent and crude topography of the time dependent ice loads during the Wisconsin glaciation. We expect that we can specify (with the aid of Quaternary Geological information) the thickness of glacial ice as a function of time (same temporal resolution as above) as averages at points on a $5^\circ \times 5^\circ$ grid for both the Laurentide and Fennoscandian ice sheets to within an accuracy which is on the order of 20 per cent absolute error at each point. The first ice model, to which we shall refer as ICE-1, is discussed in detail in Section 6. We also have to contend with the ocean loading part of the space-time dependent load redistribution process.

In principle, this part of the load history is exactly determined once the ocean function is given (Munk & McDonald 1960) since the meltwater produced by the ice sheets at each stage in the melting history must be added to the oceans in such a way that the ocean's surface remains an equipotential surface. This process is also constrained by mass conservation. The implementation of these constraints requires the inversion of an integral equation at each stage in the redistribution process (see Farrell & Clark 1976; companion paper). The kernel of this integral equation is just the Heaviside Green function for the gravitational potential perturbation given in Section 3. Its rapid inversion requires that a minimum number of ocean grid points be employed in the process. In practice, the spatial resolution of the ocean loading part of the calculation is taken to be equivalent to the resolution of the ice

sheets at points near coastlines and near the ice sheets but decreasing rapidly for mid ocean grid points which are distant from the ice centres. The grid is described in detail in Farrell & Clark (1976).

Even with the minimal spatial resolution requirements discussed above, it is quite clear that the use of a two-dimensional Simpson's Rule or any similar technique in the evaluation of (25) would be prohibitively time-consuming. What we do instead is to follow Farrell (1973) and integrate each of the Green functions required (e.g. radial displacement, gravity anomaly, gravitational potential perturbation) over circular discs of various radii α located at various distances θ from the point of observation. From these few integrations we construct a table of disc factors which can be thought of as corrections which must be applied to the Green functions when the load originates in a disc of radius α whose centre is an angular distance θ away. Now the real elements in the ice and ocean grids are not circular in shape but are normally bounded by adjacent parallels of latitude and longitude. For each such grid element the standard formulae of spherical trigonometry can be employed to find the equivalent angular radius of each of the grid elements. The error involved in this shape distortion will be small. The convolution integrals may now be found by interpolating values of the Green functions and their associated disc factors from tables. When $\alpha/\theta \gtrsim 1$, it is found sufficient to assume that the load of finite area extent originates at a point and the disc factor corrections are unnecessary. The importance of correctly determining the value of the singularity at $\theta = 0$ in the Green functions as discussed in the last section cannot be overemphasized. Failure to account properly for this will result in large errors in the vicinity of the load. This problem, however, can be easily circumvented on account of the linear time dependence of the singularity amplitude mentioned before. If we have not calculated the Green functions to sufficiently small θ values at some particular time so that the small θ asymptote is well developed, we simply make use of the known small θ asymptote to extrapolate the Green function to smaller θ in the course of computing the disc factors. This extrapolation was important only for model 2 which has the surficial low viscosity zone. In this model the singularity is much deeper than in the other two models since its rate of change of depth with time is proportional to ν^{-1} as in equation (36) and since ν^{-1} for this model is a factor of 10 larger than in the other two models. However, Model 2 is highly non-physical since the presence of the lithosphere demands an essentially infinite near surface viscosity. It will, therefore, not be employed in calculations presented here.

As an example of the disc factor corrections discussed above, we show these corrections in Fig.7 for a series of times constructed from the Heaviside Green functions for radial displacement in Model 1. When $\theta > \alpha$, the integral is divided by $G(\theta)$ to get the correction, and when $\theta < \alpha$, the integral is normalized by $G(\alpha)$. The curves for $\alpha = 0$ give the relative response for a disc load on a half space, and this is the limit towards which all of the other curves tend. Clearly from these disc factor curves the corrections are sometimes large. These large values of the correction occur when the nodal line defining the leading edge of the peripheral bulge lies near a disc edge. Then the normalization factor $G^{-1}(\theta)$ is extremely large. This may lead to large differences between adjacent entries in the table of disc factors and thus to correspondingly large errors in the interpolation between entries. Inspection of Fig. 7(d) illustrates an example of this problem. However, for Model 1 the difficulty was not encountered since the equivalent disc radii in the grid were uniformly less than $\alpha = 3°$ and inspection of Fig. 7 shows that for $\alpha \leqslant 3°$ the disc factor tables are smooth and have small variation between adjacent entries. Unfortunately the problem was encountered with Model 3 for the high viscosity lower mantle and resulted in irregularity in the computed relaxation curves at sites near the centre of the ice load. This numerical difficulty can be easily circumvented by employing a different normalization scheme for the disc factors and this approach will be taken in later work.

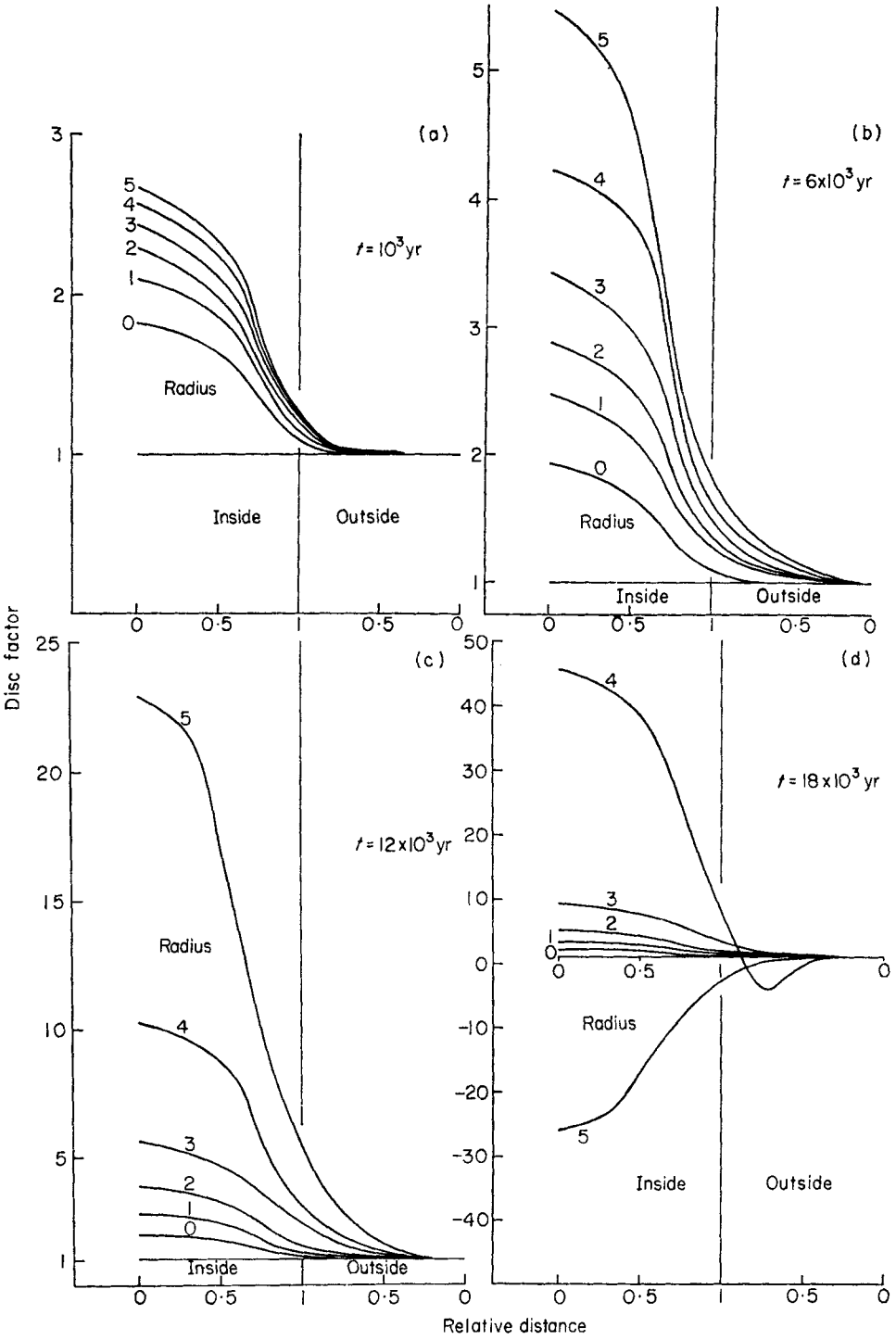

FIG. 7. (a) Disc factor curves from radial displacement Green function for Model 1 for time $t = 10^3$ yr after loading. See text for meaning of symbols. (b) Disc factor curves from radial displacement Green function for Model 1 for time $t = 6 \times 10^3$ yr after loading. (c) Disc factor curves from radial displacement Green function for Model 1 for time $t = 12 \times 10^3$ yr after loading. (d) Disc factor curves from radial displacement Green function for Model 1 for time $t = 18 \times 10^3$ yr after loading.

6. Description of a load model: Ice-1

Appendix 1 gives a tabulation of values of ice thickness on a $5° \times 5°$ grid for the Northern Hemisphere between 18 kBP, when ice sheets were, by-and-large at their maximum late Wisconsin positions and 6 kBP when all but residual ice had melted. The ice sheets thus considered in ICE-1 are the: Laurentide, Cordilleran, Greenland, Iceland, and the North European–European Arctic complex. Figs 8 and 9 represent two snapshots of the North American–Greenland glacial loads at 18 k and 10 kBP.

Three kinds of data have been used to construct maps such as Figs 8 and 9 and the list of tabulated ice thickness (Appendix 1), namely: ice margins, ice profiles, and world sea-level changes. First, several thousand radiocarbon dates have been obtained on peats, marine shells and other datable materials related in some way to the fluctuations in the margins of these late Quaternary ice sheets. For North America these data have been synthesized by Prest (1969) and Bryson (1969) as a series of maps showing isochrones (lines of equal age) on deglaciation. There are differences between these two compilations that amount to between 26 and 16 per cent variation in areal extent of the Laurentide Ice Sheet (Andrews 1973, p. 191) at different periods (e.g. $10{\cdot}65 \times 10^6\,km^2$ versus $8{\cdot}8 \times 10^6\,km^2$ at 12 000 BP). These differences are

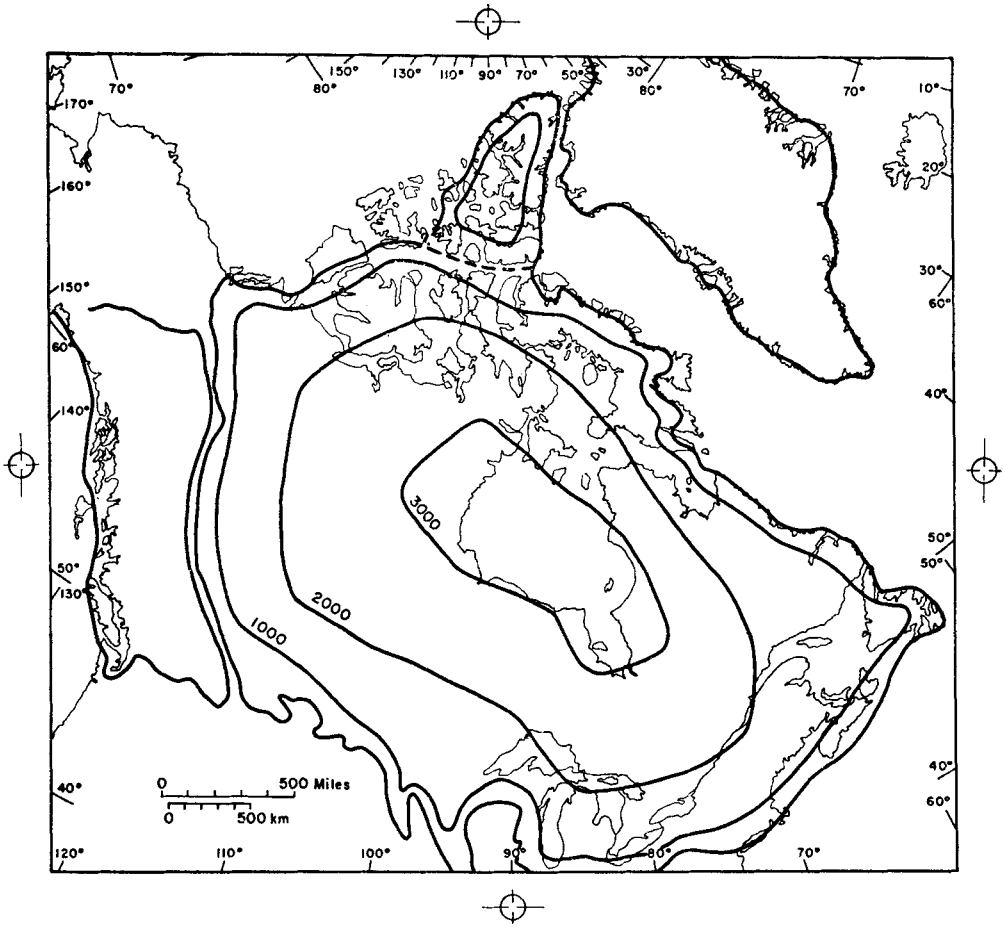

FIG. 8. Map of Laurentide ice thickness at the Wisconsin maximum approximately 18 KYBP. The Cordilleran, Innuition, and Greenland sheets are also shown.

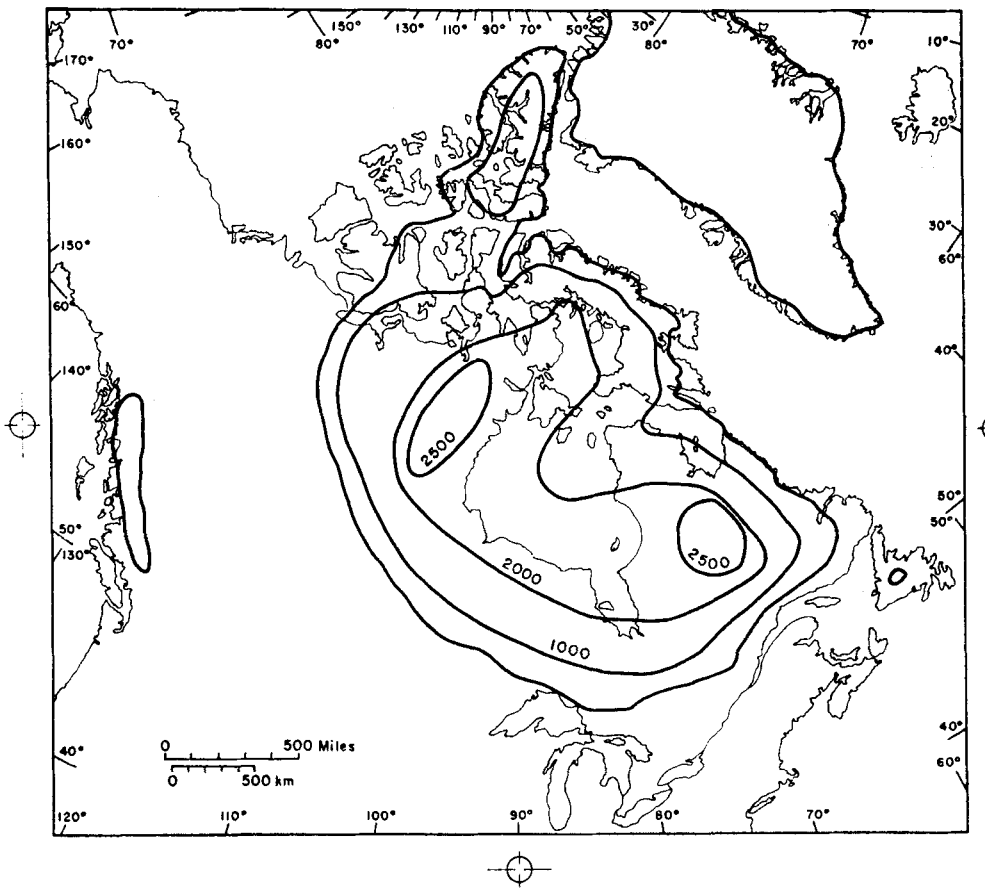

FIG. 9. Map of Laurentide ice thickness at 10 KYBP. Note the assumed splitting of the sheet into two main centres on either side of Hudson Bay by this time.

primarily caused by extrapolations across large areas where no C14 dating control is available. Prest's (1969) areas are always less than those on the Bryson *et al.* (1969) map for the same period. A tentative isochrone map at a very large scale for Europe (Zonneveld 1973) has been used for that area plus a broad knowledge of the European literature on the topic of deglaciation chronology. A major question mark surrounds the extent of glacial ice in the European–USSR arctic. Several studies (e.g. Schytt *et al.* 1968) have advanced evidence that the Barents Sea was a site for a large ice cap that actually lapped onto the northern Russian plain. There is little evidence for such a load in the pattern of postglacial uplift in northern Norway and Russia but C14 dates certainly show a broad uplift centre located over the middle of the shallow shelf that makes up the Barents Sea. Grosswald (1975, private communication) has estimated that this ice sheet and its neighbours covered a maximum area of 14×10^6 km^2—that is, larger than the Antarctic Ice Sheet today and the Laurentide at 18 k. However, the evidence is not yet compelling and in ICE-1 we have taken a conservative stance and opted for a limited ice cover over the Svalbard islands (see Appendix 1). The measure of agreement between the amplitude of our predicted recovery and that observed will provide a first measure of the accuracy of our prediction of the extent of this ice sheet. In ICE-1 we have ignored the effects caused

by the build-up and deglaciation of ice masses in the Southern Hemisphere. One significant unknown is the extent of ice in Antarctica about 18 k. This situation is being rapidly corrected (e.g. Fig. 1 in Hughes 1975).

The second step in the construction of ICE-1 is to provide reasonable estimates of ice thickness at each grid point. This is equivalent to reconstructing the late Quaternary ice sheets as in Figs 8 and 9. Paterson (1972) has recently provided a comprehensive review of the equations and assumptions necessary to reconstruct ice sheet profiles and hence, ice thickness. One unknown, however, is the amount of isostatic compensation at various points under the ice sheets. Some reasonable estimates can be made, however, by considering equilibrium deflections on a spherical two-layered, two-dimensional earth (cf. Brotchie & Silvester 1969). The problem of reconstructing ice thickness is, however, significantly more complex than the physics of the situation suggests. Although good estimates can be made of ice sheets that are radially symmetric and with a single-ice centre the computational problem becomes large if there is reason to believe that significant shifts occurred in the geographical location of the major outflow centres. For the Laurentide Ice Sheet this is now thought to be the case and such a model is required to explain the catastrophic deglaciation of much of Hudson Bay in a matter of a few hundred years (Andrews & Falconer 1969). Thus, in Fig. 9 and in Appendix 1 we allow the Hudson Bay ice divide to collapse and migrate between 18 and 8 k (Andrews & Peltier submitted). Thus, our ice thickness estimates (Appendix 1) use reasonable equations for the relation between distance from the ice margin and ice thickness as well as our best estimate on the history of the critical central areas. In terms of maximum ice thickness we have followed Paterson (1972) who estimated approximately 3500 m for the Laurentide Ice Sheet. This is similar to that for present day Greenland and rather less than the 4000 m + for Antarctica.

A first-order check on the *volume* of ice contained in ICE-1 is contained in the numerous estimates of changes in world sea-level over the last 18 k. ICE-1 can be represented in an integral sense as an equivalent amount of water released to the oceans as a function of time. Although there are severe difficulties in establishing *the* glacio-isostatic sea level curve to which this equivalent must conform (see Farrell & Clark 1976, companion paper), nevertheless, the progressive rise of world sea level due to deglaciation after $t = 18$ kBP is known within certain error limits.

Fig. 10 shows our mean sea level history based upon ICE-1; we reiterate that we have not included in ICE-1 the ice sheets of the Southern Hemisphere or the smaller ice caps and glaciers in the north such as the Alps. Thus, our estimate of global sea-level rise (more correctly its mass equivalent) is an underestimate. ICE-1 contains a mass equivalent to a 77-m rise in global sea level at 18 kBP, a figure which is not far removed from the upper limit of 80–100 m considered to represent the net sea-level rise during the late Wisconsin glaciation (cf. Mörner 1971, Fig. 4). On Fig. 10 we contrast our mean sea-level history with the generalized eustatic curve of Shepard (1963). Our curve lies consistently below the latter with a difference of approximately 10 m. Part of this difference may be caused by our underestimation of the ice load, but it is certainly also due in part to isostatic effects not accounted for in Shepard's curve due to the lack of an absolute datum with which to compare. This ambiguity can be entirely resolved by application of the methods discussed by Farrell & Clark (1976, companion paper).

7. Comparisons of observation and theory

To the extent that sea level may be considered absolutely stationary at times sufficiently long after deglaciation equation (25) with L described by (26) determines the relative sea-level curve at a point (θ, λ) on the Earth's surface. As stated previously, L should contain both the ice and ocean parts of the surface mass load. However, sufficiently near the glaciated regions the response will be dominated by the deglacia-

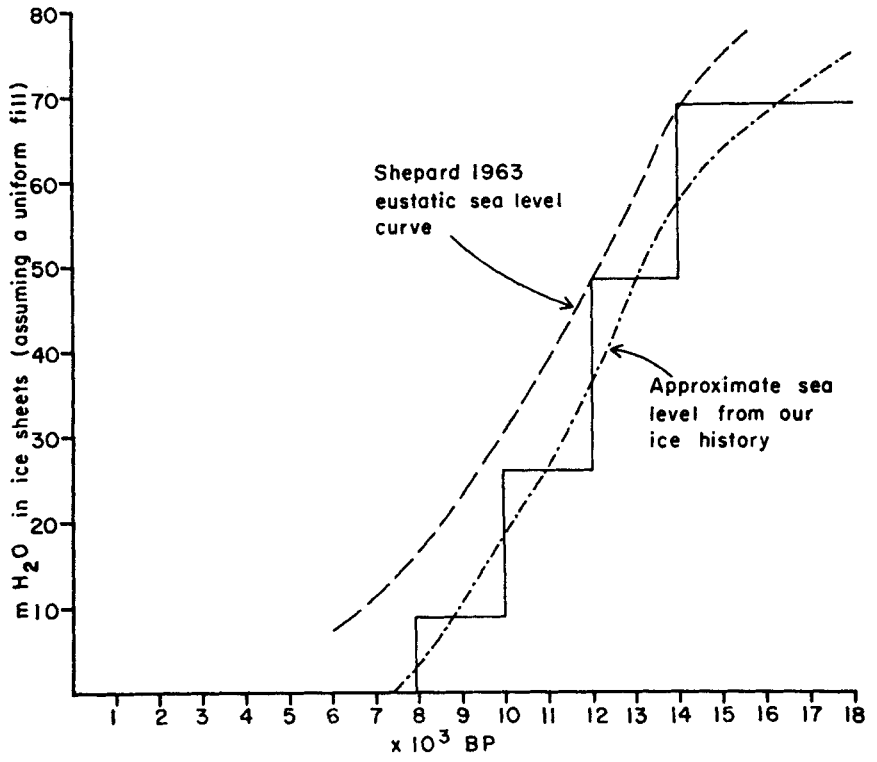

FIG. 10. Mean sea level history for ICE-1 contrasted with Shepard's (1963) generalized eustatic curve.

tion itself and the ocean loading should introduce but a small correction. In this section we will compute relaxation curves according to (25) and with a single exception will neglect the loading of the ocean basins entirely. As shown by Farrell & Clark (1976, companion paper) this may lead to significant error even in the vicinity of the load since sea level is held anomalously high in the northern Atlantic and Pacific Oceans on account of the direct gravitational attraction of the ice. Whether this will produce a detectable signal in the relaxation curves long after deglaciation has been completed will require further calculation to elucidate. Here, we will restrict ourselves to examination of the simplest possible signature of the response and will attempt to isolate certain systematic differences between observations and the predictions of theory. Certain of these systematic errors may be ascribed to errors in ICE-1 while others are unambiguously related to errors in the visco-elastic model.

The sites which we have selected for comparison of theory and observation are shown on the location map in Fig. 11. They were chosen on the basis of availability of good quality C 14 data but do not exhaust the list of sites at which data of such quality is available. Our data sources for these sites are included in the detailed site description given in Appendix 2. Using ICE-1 we compute $\Delta R(\theta, \lambda, t)$ according to (25) using G_R appropriate to Model 1 (uniform viscosity mantle with $\nu = 10^{22}P$) and G_R appropriate to Model 3 (high viscosity lower mantle with $\nu = 10^{24}P$ below a depth of 10^3 km and $\nu = 10^{22}P$ in the upper mantle). Neither of these models have a lithosphere so that one of the systematic errors we hope to find should be due to the absence of this well-documented characteristic of the planet. In the lithosphere ν is essentially infinite. The thickness of this surface lid should be on the order of 100 km with perhaps some lateral variation of thickness between continental and oceanic

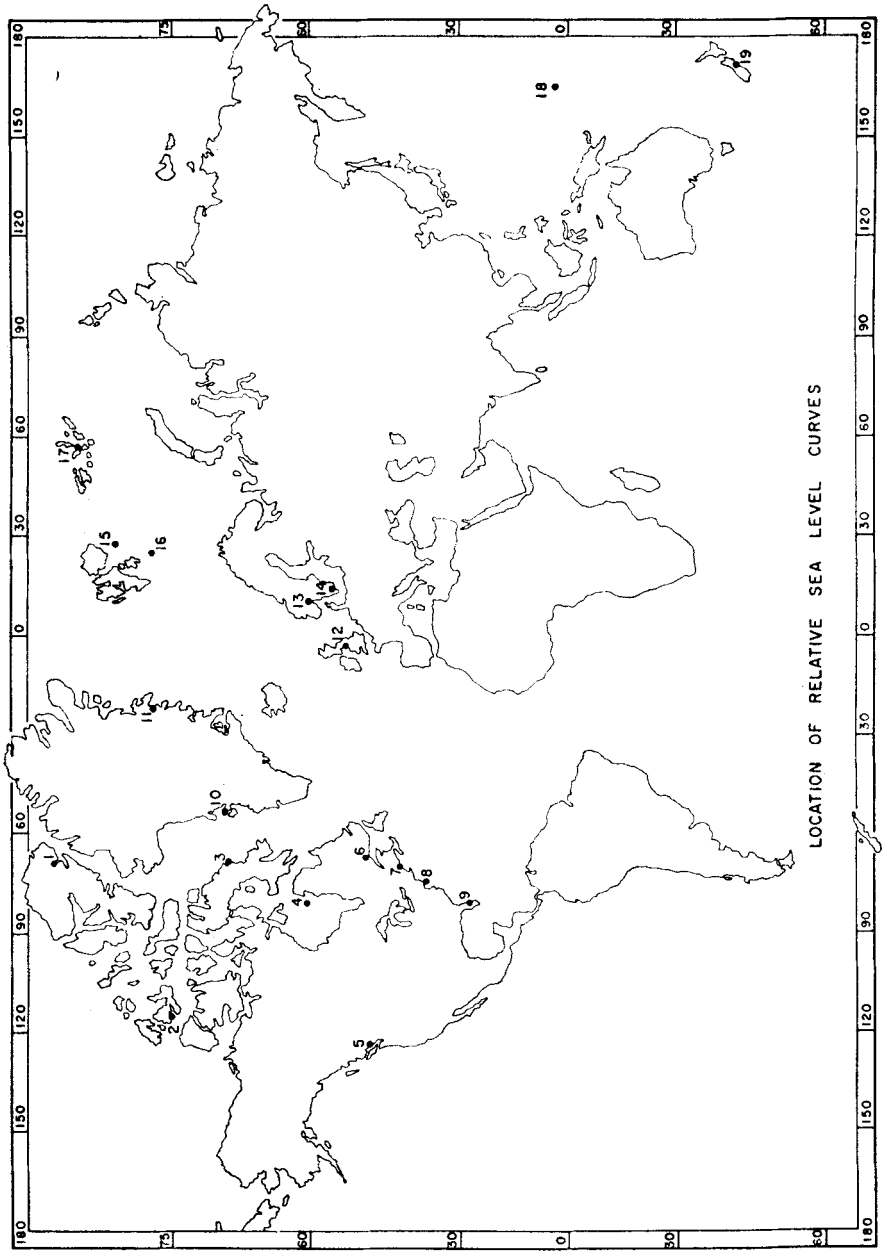

FIG. 11. Location map for sites of relaxation data selected for comparison of theory of observation. The sources of the data at these sites are given in an abbreviated list of references at the end of the main bibliography.

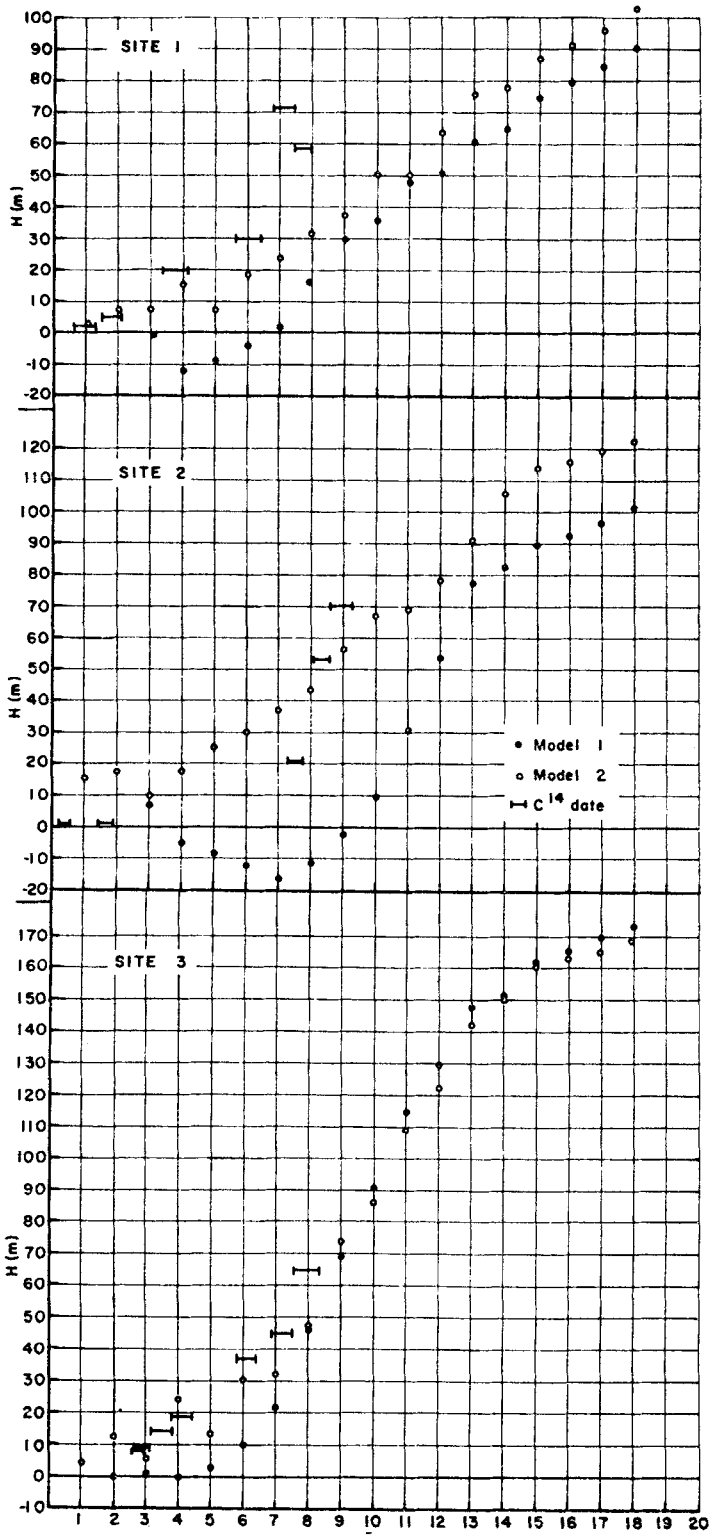

FIG. 12. Relaxation data (C14 dates and elevations) at sites 1–3 compared with predictions of viscosity models 1 and 3 of Fig. 1. Model 2 on this and the ensuing figures corresponds to viscocity Model 3. Site numbers as shown.

regions. As shown in Paper 2 and by previous authors (e.g. McConnell 1963) the effect of the lithosphere on relaxation spectra is to *decrease* the decay time for short deformation wavelengths. Since short deformation wavelengths will have large amplitude only near the edge of an ice sheet we can expect to find indications of the presence of the lithosphere in data from such regions. Qualitatively the effect should be such that edge located relaxation curves have a much shorter relaxation time than predicted either from Model 1 or from Model 3. We will see that this is, in fact, the case. The sites shown in Fig. 11 are discussed in detail in Appendix 2.

Here, we will lump the sites into three geographical bins for the purpose of general discussion. Sites numbered 1, 2, 5, 6, 7, 10, 11 are 'edge sites', i.e. near the initial edge of the ice sheets. Sites numbered 3, 4, 13, 14 are 'central sites' although 3 and 13 are somewhat nearer the edge of the Laurentide and Fennoscandian ice sheets respectively than are 4 and 14. Sites 8, 9, 18 and 19 are peripheral sites (i.e. far removed from the ice-sheet edges in the ice-free region) although 8 is much closer to an edge than the other three. Figs 12, 13, 14 and 15 show the comparison of observed relaxation data with those predicted by the theory for viscosity Models 1 and 3. Note in the figures that the first viscosity model is labelled 1 and the third viscosity model is labelled 2. Model 3 includes ocean basin filling on viscosity Model 1 and has been calculated only for site 9.

Inspection of the relaxation curves from edge sites illustrates the large systematic errors in relaxation time between those predicted by either viscosity Model 1 or viscosity Model 3 and those observed. These systematic errors are in the sense described above and are thus indicative of the presence of the lithosphere. At edge sites the relaxation times are anomalously short. Later versions of the visco-elastic model will require a lithosphere lid in order to fit these data. Since most relaxation data are from edge sites for obvious geographical reasons we expect that a proper inversion of them will provide interesting information upon lateral variations in lithospheric thickness.

At sites near the ice-sheet centres (4 and 14 in particular) the predictions of viscosity Model 1 are in near perfect accord with the observations. At these same sites viscosity Model 3 predicts a much higher present-day rate of uplift than that which is observed so that high lower mantle viscosity is effectively excluded if a Maxwell rheology is assumed.

This conclusion is strongly reinforced by relaxation data from peripheral sites, particularly that for the Florida region (site 9). Viscosity Model 1 fits the data with high accuracy whereas viscosity Model 3 (labelled 2 in the figure) predicts current uplift of that region—entirely the opposite of what is observed.

The initial solutions of the forward problem which we have obtained strongly suggest that the global set of relative sea-level curves are invertable in terms of a simple radially stratified Maxwell model of the interior. They furthermore suggest that a good first guess viscosity profile for such inversion would consist of a mantle with a uniform viscosity of 10^{22} Poise (cgs) capped by a lithosphere lid with infinite viscosity having a thickness which is on the order of 100 km. The theory which shall be employed in this inversion is detailed in the companion paper (Paper 2).

In Appendix 2 a detailed description of the comparison of theory and observation at each of the 19 sites which we have examined is given. Appended to the main reference list of the paper is a list of references to the sources which we have used for the observed relaxation data at each site.

8. Conclusions

We have described our first attempt to demonstrate the detailed compatibility between a linear visco-elastic (Maxwell) model of the planetary interior and a global set of relative sea-level curves pertaining to the last major glaciation event on the

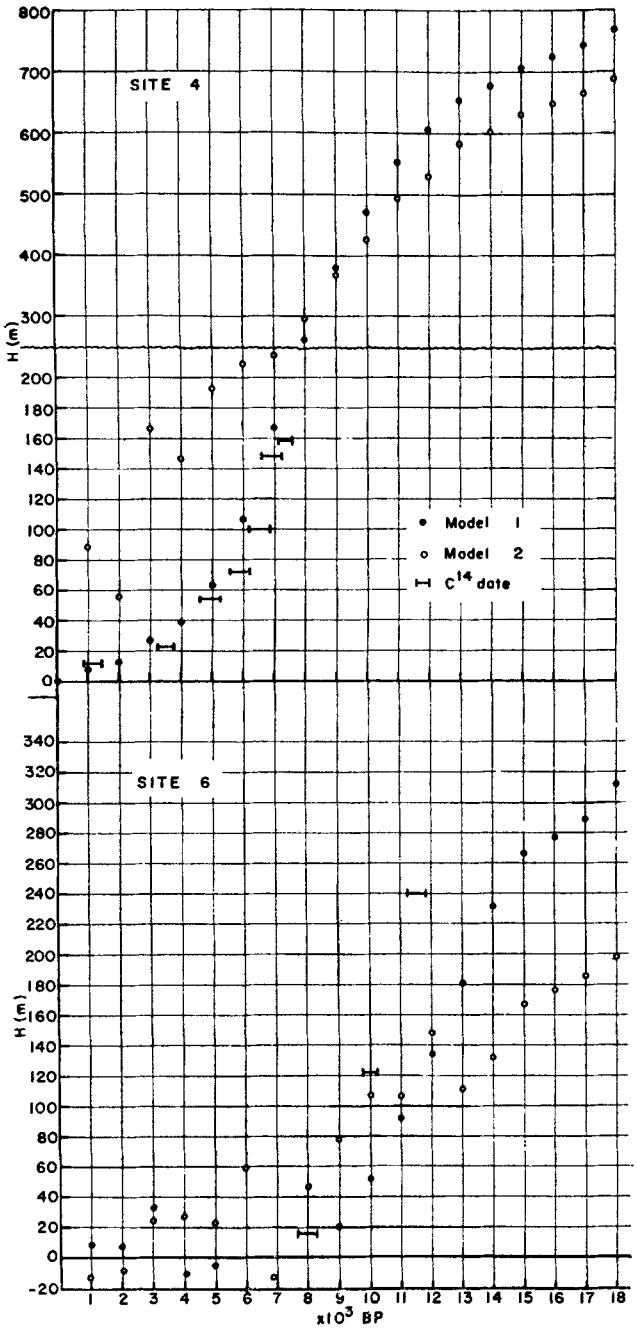

FIG. 13. Relaxation data at sites 4–7 compared with theoretical predictions from viscosity Models 1 and 3. Site numbers as shown.

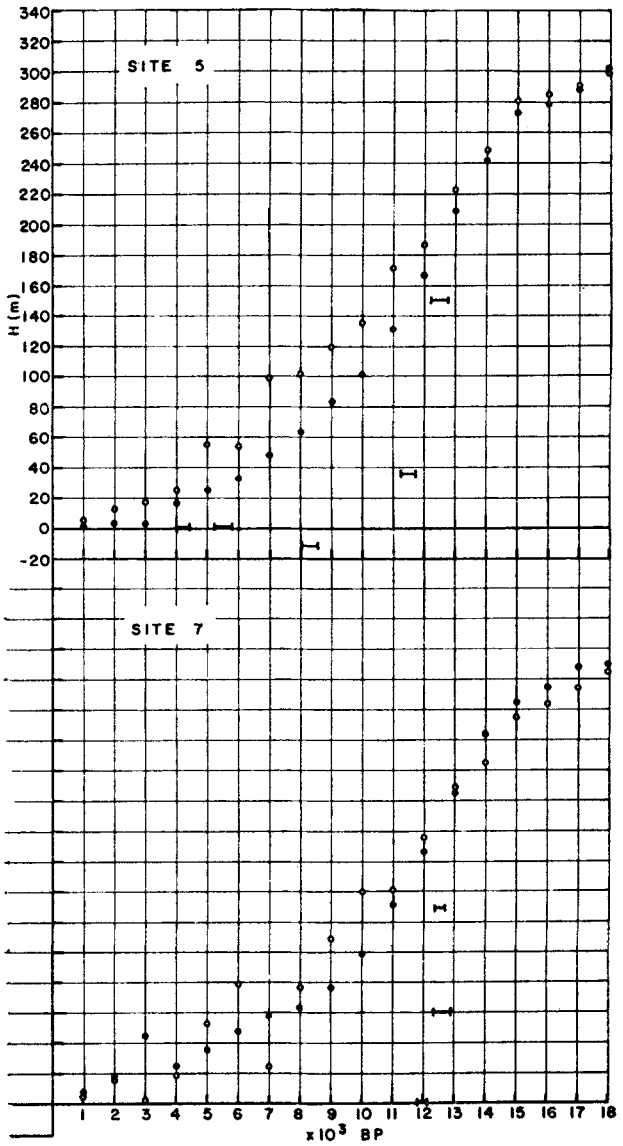

FIG. 13. Relaxation data at sites 4–7 compared with theoretical predictions from viscosity Models 1 and 3. Site numbers as shown.

Earth's surface. We believe that for a first attempt it has been remarkably successful. These detailed comparisons of theory and observation have, however, pointed to several inadequacies of the model which must be corrected before complete compatibility can be claimed. In spite of these inadequacies we believe that one important conclusion is well justified. This is that the lower mantle cannot have a viscosity which is significantly in excess of that in the upper mantle. If the lower mantle has a high viscosity (say $\nu = 10^{24}P$ in the lower 2×10^3 km) then the present-day rates of uplift would be much higher than they are observed to be near the ice-sheet centres. In addition, the sense of the rebound at sites sufficiently removed from the ice-sheet centre would be reversed from that which is observed (e.g. Florida would be rising at

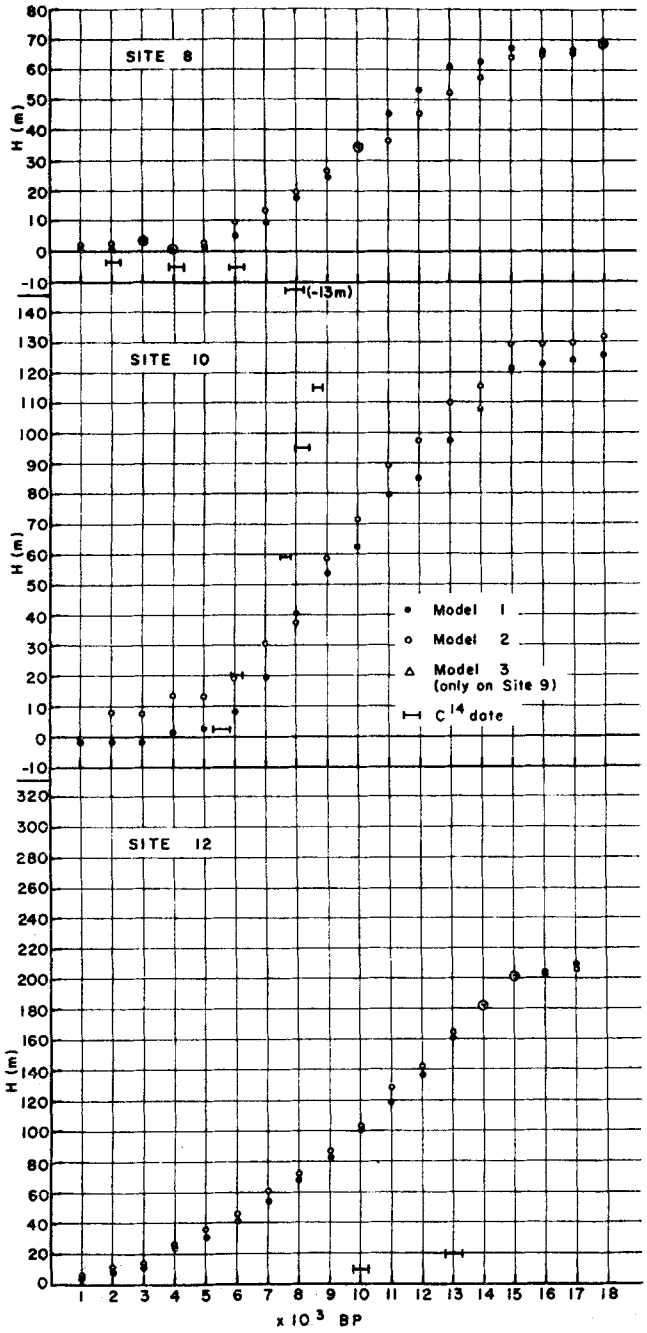

FIG. 14. Relaxation data at sites 8–13 compared with theoretical predictions from viscosity Models 1 and 3. Site numbers as shown. Note Model 3 on site 9 includes ocean basin filling on viscosity Model 1. For this calculation it was assumed that the ocean basins filled uniformly.

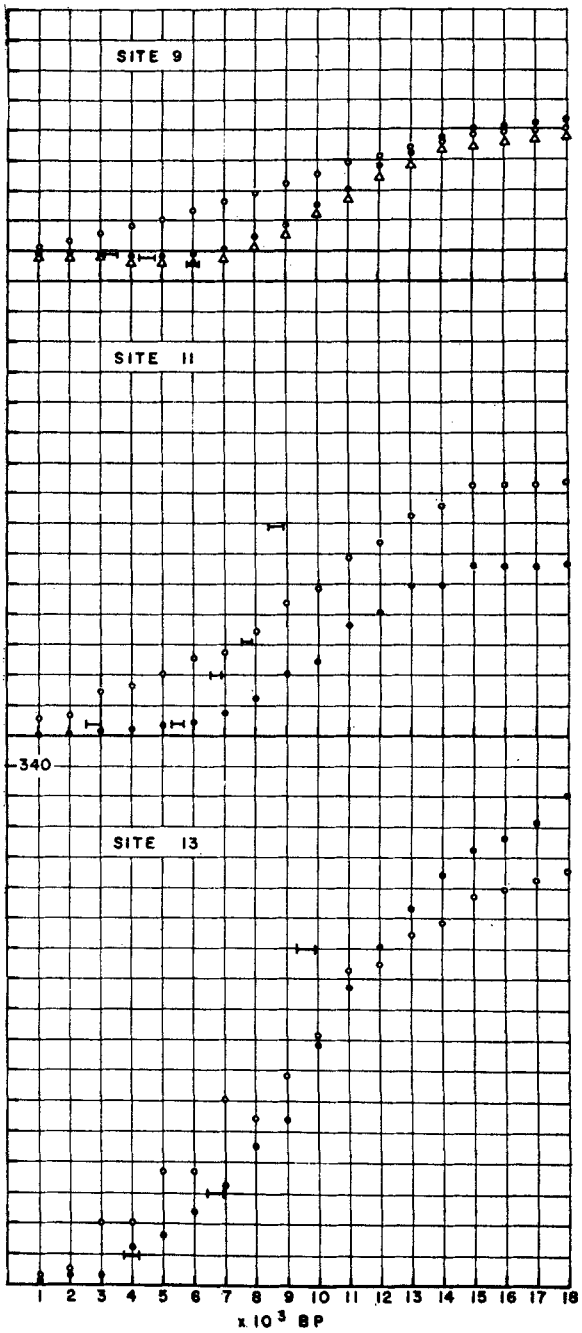

FIG. 14. Relaxation data at sites 8–13 compared with theoretical predictions from viscosity Models 1 and 3. Site numbers as shown. Note Model 3 on site 9 includes ocean basin filling on viscosity Model 1. For this calculation it was assumed that the ocean basins filled uniformly.

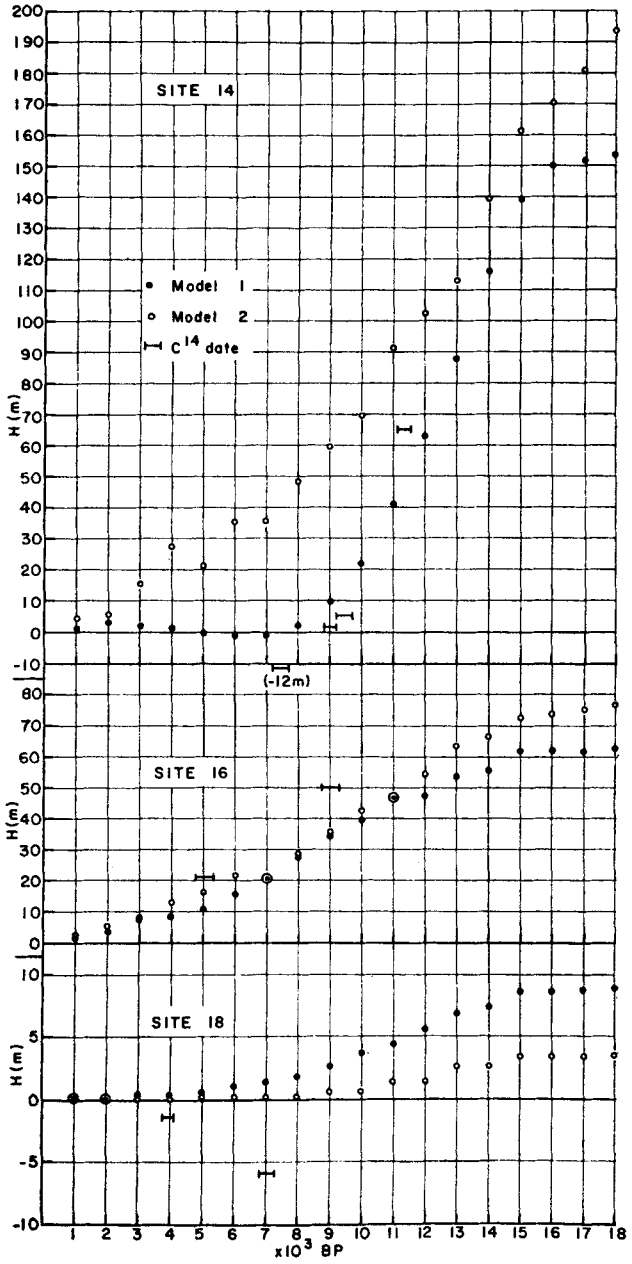

FIG. 15. Relaxation data at sites 14–19 compared with theoretical predictions from viscosity Models 1 and 3. Site numbers as shown.

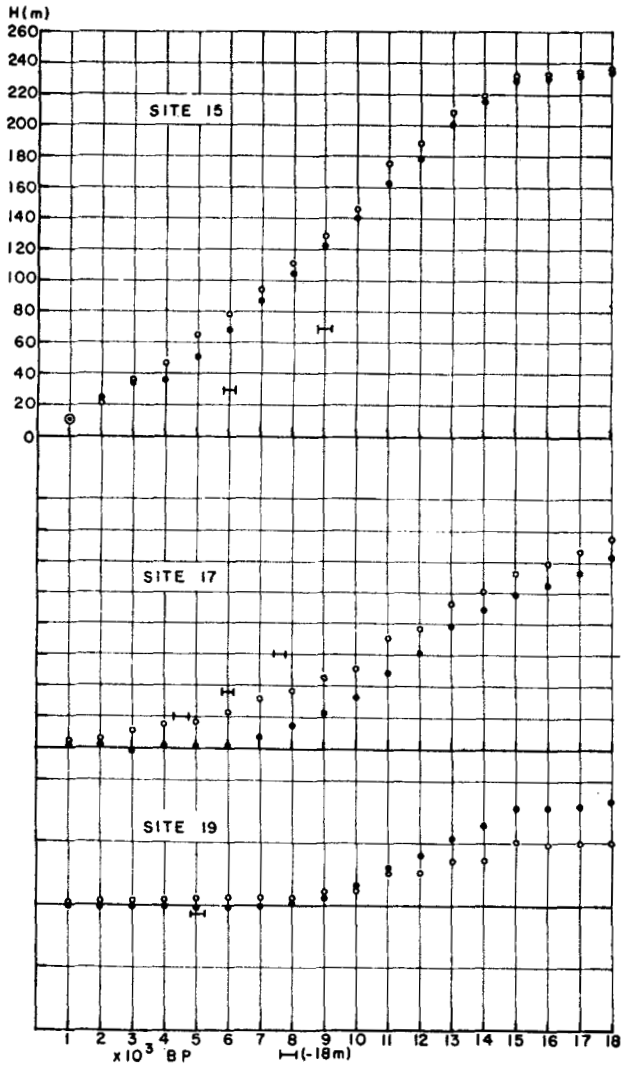

FIG. 15. Relaxation data at sites 14–19 compared with theoretical predictions from viscosity Models 1 and 3. Site numbers as shown.

present whereas the observation demands sinking). This conclusion and the basis of it is in accord with that reached by Cathles (1971, 1975) on the basis of a spectral model of the adjustment process. Since the numerical structure of the two calculations is entirely different, yet the conclusions the same, we believe that the conclusion is strongly reinforced. The theoretical explanation for the apparent dichotomy between this conclusion based upon an analysis of isostatic adjustment with a spherical self-gravitating model and the opposite conclusion reached earlier by McConnell (1963) using a plane earth model is given in Paper 2. It is connected with the fact that the spherical models support the existence of certain core modes of viscous gravitational relaxation; modes which may be significantly excited by the disintegration of a moderate sized ice sheet.

In addition to this main conclusion we have shown clearly that the influence of the lithosphere is readily apparent in most if not all relaxation curves from sites near the edge of the main Wisconsin ice sheets. The incorporation of the lithosphere in visco-elastic models of the interior is thus of fundamental importance if these models are to be made compatible with the observed relaxation data. As seen in the last section the systematic errors are sufficiently large in the absence of this feature that the relaxation data set should prove highly diagnostic of lithospheric thickness. It should subsequently prove possible to determine quantitatively the extent of the lateral variation of this parameter by inverting the edge data according to geographical location. The theoretical basis of the inverse problem for mantle viscosity is developed in Paper 2.

We have seen in the previous section that there are certain inadequacies of ICE-1 which will also require rectification if we are to proceed towards the application of the formal inverse theory described in Paper 2. In certain regions in which the Quaternary data is inadequate we have shown that the phase of load removal (i.e. timing) is incorrect. In other regions the mass itself is not compatible with local rebound histories (e.g. the Barents Sea region). In addition, the total mass influx to the oceans may be too low (by $\approx$ 10 per cent). These first refinements of ICE-1 will be incorporated into a new load model ICE-2. As discussed in 2 we shall proceed iteratively to refine simultaneously our knowledge of the load $L(\theta, \lambda)$ and of the viscosity profile $v(r)$. We are forced to proceed iteratively since the full inverse problem is a non-linear one.

We have furthermore identified a source of error in the numerical structure of the model itself. A new normalization scheme for the disc factor tables employed in doing the two-dimensional convolutions is required. This is a simple problem to circumvent and will not trouble us in future calculations.

The pursuit of such calculations as those presented here may be expected to contribute substantially to our understanding of the rheological behaviour of the planet. The implications of the conclusion that the effective viscosity of the mantle is substantially uniform are of obvious importance to the understanding of the mantle general circulation. If some form of thermal convection drives the motion of surface plates then the effective viscosity of the fluid is critical in determining the time scale of the circulation. Furthermore, the depth dependence of this parameter (if any) influences the spatial dimensions of the quasi-cellular flow. These dimensions may be on observable.

We may furthermore expect that these calculations will provide a firm theoretical foundation upon which the interpretation of Quaternary geological data may be based. For example, we can expect to learn a great deal more than we know at present concerning the distribution of ice on the Earth's surface during the last glacial epoch. Given this refined knowledge of the time dependent distribution of the glacial ice we will be able to calculate exactly the space and time dependent rise of global sea level.

It cannot be emphasized strongly enough that the calculations described here should be regarded as preliminary. We expect that several of our tentative conclusions will require later modification as we accrue further experience in modelling signatures of the isostatic adjustment process. For instance, incorporation of the self- consistent ocean filling calculation in the model should drastically alter our preliminary picture of adjustment at sites remote from the main ice sheet centres, and for times within the period of active deglaciation.

Acknowledgments

Most of this study was completed during a visiting appointment of one of us (WRP) at CIRES and INSTAAR in Boulder, Colorado during the summer of 1974.

WRP is grateful to both of these institutions for helping to make the visit an enjoyable and productive one. W. E. Farrell generously provided a copy of his convolution routine for the ocean tidal loading problem, which, although it required some modification for the present application made it possible to complete the calculations more quickly than would otherwise have been the case. We have enjoyed useful discussions with him and with J. Clark on the subject of this paper.

References

Alterman, Z., Jarosch, H. & Pekeris, C. L., 1961. Propagation of Rayleigh Waves in the Earth, *Geophys. J. R. astr. Soc.*, **4**, 219.

Andrews, J. T., 1969. Importance of the radiocarbon standard deviation in determining relative sea levels and glacial chronology from east Baffin Island, *Arctic*, **22**, 13–24.

Andrews, J. T., 1970. Postglacial uplift in Arctic Canada, *Sepc. Publ. No.* 2, *Inst. Br. G.*, 156 pp.

Andrews, J. T., 1973. The Wisconsin Ice Sheet: dispersal centres, problems of rates of retreat, and climatic implications, *Arctic Alpine Res.*, **5**, 185–200.

Andrews, J. T., 1974. *Glacial isostasy*, Dowden, Hutchinson and Ross, Inc., Stroudsburg, Pennsylvania, USA.

Andrews, J. T. & Falconer, G., 1969. Late glacial and postglacial history and emergence of the Ottawa Islands, Hudson Bay, N.W.T.: evidence on the deglaciation of Hudson Bay. *Can. J. earth Sci.*, **6**, 1263–1276.

Backus, G. E., 1967. Converting vector and tensor equations to scalar equations in spherical co-ordinates, *Geophys. J. R. astr. Soc.*, **13**, 71.

Backus, G. E. & Gilbert, J. F., 1967. Numerical applications of a formalism for geophysical inverse problems, *Geophys. J. R. astr. Soc.*, **13**, 247.

Backus, G. E. & Gilbert, J. F., 1968. The resolving power of gross earth data, *Geophys. J. R. astr. Soc.*, **16**, 169.

Backus, G. E. & Gilbert, J. F., 1970. Uniqueness in the inversion of inaccurate gross earth data, *Phil. Trans. R. Soc. Lond.*, **A 266**, 123.

Bloom, A. L., 1967. Pleistocene shorelines: A new test of isostasy, *Bull. geol. Soc. Am.* **78**, 1477.

Brennan, C., 1974. Isostatic recovery and the strain rate dependent viscosity of the earth's mantle, *J. geophys. Res.*, **79**, 3993.

Brotchie, J. F. & Silvester, R., 1969. On crustal flexure. *J. geophys. Res.*, **74**, 5240–5252.

Bryson, R. A., Wendland, W. M., Ives, J. D. & Andrews, J. T., 1969. Radiocarbon isochrones on the disintegration of the Laurentide Ice Sheet, *Arctic Alpine Res.*, **1**, 1–14.

Cathles, L. M., 1971. *The viscosity of the Earth's mantle*, PhD thesis, Princeton University, New Jersey, USA.

Cathles, L. M., 1975. *The viscosity of the Earth's mantle*, Princeton University Press, New Jersey, USA.

Dicke, R. H., 1966. The secular acceleration of the earth's rotation, *The Earth–Moon System*, p. 98, ed. B. G. Marsden and A. G. W. Cameron, Plenum Press, New York.

Dicke, R. H., 1969. Average acceleration of the earth's rotation and the viscosity of the deep mantle, *J. geophys. Res.*, **74**, 5895.

Farrell, W. E., 1972. Deformation of the earth by surface loads, *Rev. geophys. space Phys.*, **10**, 761.

Farrell, W. E., 1973. Earth tides, ocean tides, and tidal loading, *Phil. Trans. R. Soc. Lond.*, **A 274,** 45.

Farrell, W. E. & Clark,, J. A. On postglacial sea level, *Geophys. J. R. astr. Soc* **46,** 647–667.

Gilbert, F. & Dziewonski, A., 1975. An application of normal mode theory to the retrieval of structural parameters and source mechanisms from seismic spectra, *Phil. Trans. R. Soc. Lond.*, **A 278,** 187.

Goldreich, P. & Toomre, A., 1969. Some remarks on polar wandering, *J. geophys. Res.*, **74,** 2555.

Gordon, R. B., 1965. Diffusion creep in the earth's mantle, *J. geophys. Res.*, **70,** 2413.

Gordon, R. B., 1967. Thermally activated processes in the earth: Creep and seismic attenuation, *Geophys. J. R. astr. Soc.*, **13,** 33.

Haskell, N. A., 1935. The motion of a viscous fluid under a surface load, 1, *Physics*, **6,** 265.

Haskell, N. A., 1936. The motion of a viscous fluid under a surface load, 2, *Physics*, **7,** 56.

Haskell, N. A., 1937. The viscosity of the asthenosphere, *Am. J. Sci.*, **33,** 22.

Hughes, T., 1975. The West Antarctic Ice Sheet: instability, disintegration, and initiation of Ice Ages, *Rev. geophys. space Phys.*, **13,** 502–526.

Kaula, W. M., 1963. Elastic models of the mantle corresponding to variations in the external gravity field, *J. geophys. Res.*, **68,** 4967.

Kaula, W. M., 1972. Global gravity and tectonics, in *The nature of the solid Earth*, p. 335, ed. E. C. Robertson, McGraw–Hill, New York.

Kuo, J. T., 1969. Static response of a multilayered medium under inclined surface loads, *J. geophys. Res.*, **74,** 3195.

Longman, I. M., 1962. A Green's function for determining the deformation of the earth under surface mass loads, 1, Theory, *J. geophys. Res.*, **67,** 845.

Malvern, L. E., 1969. *Introduction to the mechanics of a continuous medium*, Prentice–Hall, Inc., Englewood Cliffs, New Jersey.

McConnel, R. K., 1963. *The visco-elastic response of a layered earth to the removal of the Fennoscandian ice-sheet*, PhD thesis, University of Toronto, Toronto.

McKenzie, D. P., 1966. The viscosity of the lower mantle, *J. geophys. Res.*, **71,** 3995.

McKenzie, D. P., 1967. The viscosity of the mantle, *Geophys. J. R. astr. Soc.*, **14,** 297.

McKenzie, D. P., 1968. The geophysical importance of high temperature creep, in *The history of the Earth's crust*, ed. R. A. Phinney, Princeton University Press, Princeton, New Jersey.

McKenzie, D. P., Roberts, J. M. & Weiss, N. O., 1974. Convection in the earth's mantle: Towards a numerical simulation, *J. Fluid Mech.*, **62,** 465.

Munk, W. H. & MacDonald, J. F., 1960. *The rotation of the Earth*, Cambridge University Press, New York.

Niskanen, E., 1948. On the viscosity of the earth's interior and crust, *Ann. Acad. Sci. Fenn., Ser. A*, **3** (15), 22.

O'Connell, R. J., 1971. Pleistocene glaciation and the viscosity of the lower mantle, *Geophys. J. R. astr. Soc.*, **23,** 299.

Parsons, B. E., 1972. *Changes in the earth's shape*, PhD thesis, Cambridge University, Cambridge.

Paterson, W. S. B., 1972. Laurentide ice sheet: Estimated volumes during late Wisconsin, *Rev. geophys. space Phys.*, **10,** 885.

Peltier, W. R., 1972. Penetrative convection in the planetary mantle, *Geophys. Fluid Dyn.*, **3,** 265.

Peltier, W. R., 1974. The impulse response of a Maxwell earth, *Rev. geophys. space Phys.*, **12,** 649.

Peltier, W. R., 1976. Glacial isostatic adjustment—II, The inverse problem, *Geophys. J. R. astr.Soc.* **46,** 000.
Prest, V. K., 1969. Retreat of Wisconsin and Recent ice in North America, *Geol. Surv. Canada,* Map 1257A.
Schytt, V., Hoppe, G., Blake, W. & Grosswald, M. G., 1968. The extent of Würm glaciation in the European Arctic, *Bull. Int. Assoc. Sci. Hydrol.*, **79,** 207–216.
Shepard, F. P., 1963. Thirty-five thousand years of sea level, *Essays in Marine Geology,* University Southern California Press, 1–10.
Shepard, F. P. & Curray, J. R., 1967. Carbon-14 determination of sea level changes in stable areas, in *Progress in Oceanography,* ed. M. Sears, Pergamon Press, Inc., New York.
Vening Meinesz, F. A., 1937. The determination of the earth's plasticity from post-glacial uplift of Fennoscandia: Isostatic adjustment, *Proc. Kon. Ned. Akad. Wetensch,* **40,** 654.
Walcott, R. I., 1972a. Quaternary vertical movements in eastern North America: Quantitative evidence of glacio-isostatic rebound, *Rev. Geophys. Space Phys.*, **10,** 849.
Walcott, R. I., 1972b. Past sea levels, eustasy and deformation of the earth, *Quaternary Res.*, **2,** 1.
Weertman, J., 1970. The creep strength of the earth's mantle, *Rev. Geophys. Space Phys.*, **8,** 145.
Zonneveld, J. I. S., 1973: Some notes on the last deglaciation in Northern Europe compared with Canadian Conditions, in Symposium Discussion, *Arctic Alpine Res.*, **5,** 223–228.

Abbreviated References to data sources for sites on Fig. 11

Site 1. England, J. H., 1974. PhD thesis, University of Colorado. England, J. H., 1976. *Arctic and Alpine Rès.*, in press.
Site 2. Henoch, W. E. S., 1974. *Geogr. Bull.*, **22,** 105–126.
Site 3. Løken, O. H., 1965. *Geogr. Bull.*, **7,** 243–258.
Site 4. Andrews, J. T. & Falconer, G., 1969. *Can. J. earth Sci.*, **6,** 1263–1276.
Site 5. Matthews, E. H. *et al.* 1970. *Can. J. earth Sci.*, **7,** 690–702.
Site 6. Elson, J. A., 1969. *Rev. Geogr. Montreal,* **23,** 247–258.
Site 7. Stuiver, M. & Borns, H. W., 1975. *Bull. geol. Soc. Am.*, **86,** 99–104.
Site 8. Stuiver, M. & Daddario, J. J., 1963. *Science,* **142,** 951.
Site 9. Scholl, D. W. F. *et al.*, 1969. *Science,* **163,** 562–564.
Site 10. Ten Brink, N. W. 1974. *Bull. geol. Soc. Am.*, **85,** 219–228. Kelly, M., 1973. Grønlands, *Geol. Unders. Rapp.* **Nr. 59.**
Site 11. Washburn, A. L. & Stuiver, M., 1962. *Arctic,* **15,** 66–73. Lasca, N. P., 1966. *Arctic,* **19,** 349–353.
Site 12. Andrews, J. T. *et al.*, 1973. *Geol. en Mijnbouw,* 52–1–12. Tooley, M. J., 1974. *Geogr. J.*, **140,** 18–42.
Site 13. *in* Kenney, T. C., 1964. *Géotechnique,* **14,** 203–230.
Site 14. Mörner, N-A., 1969. *Geol. en Mijnbouw,* **48,** 389–399.
Site 15. Schytt *et al.*, 1968. *Bull. Int. Assoc. Sci. Hydrol.*, **79,** 207–216.
Site 16. Schytt *et al.*, 1968—as for site 15.
Site 17. Grosswald, M., 1972. *Acta Univ. Olu,* Finland, Ser. A., Geol. No. 1, 205–224.
Site 18. Bloom, A. L., 1970. *Bull. geol. Soc. Am.*, **81,** 1895–1905.
Site 19. Schofield, J. C., 1964. *N. Z. J. Geol. Geophys.*, **7,** 359–370.

Appendix 1

Ice-1 load history

Laurentide Ice

Colat	E-Long	18	14	12	10	8	6
10	265	500	300	200	200	0	0
10	270	1000	850	800	800	900	500
10	275	2000	1250	1200	1200	500	0
10	280	2000	1250	1200	1200	1000	500
10	285	1000	650	600	600	200	500
10	295	500	0	0	0	100	0
10	300	1000	1000	500	500	900	500
10	305	1500	1450	1200	1200	1450	1000
10	310	1500	1450	1200	1200	1450	1400
10	315	2000	2000	1950	1950	1950	2000
10	320	2200	2150	2100	2050	2000	1900
10	325	2500	2450	2400	2350	2250	2150
10	330	2200	2150	2050	2000	1800	1600
10	335	1500	1400	1300	500	0	0
15	250	200	300	300	0	0	0
15	255	200	1000	1000	0	0	0
15	260	1000	1400	1400	0	0	0
15	265	1000	1500	1500	600	0	0
15	270	1000	1200	1200	900	700	0
15	270	1000	900	800	800	900	500
15	280	0	200	100	100	0	0
15	305	1000	900	600	500	900	500
15	310	2000	2000	2000	1950	1900	1900
15	315	2700	2700	2700	2650	2650	2700
15	320	2800	2750	2700	2650	2600	2500
15	325	3000	2950	2900	2850	2800	2700
15	330	3000	2950	2900	2850	2800	2700
15	335	2000	1950	1900	1800	1500	1300
20	235	10	300	300	0	0	0
20	240	1200	1400	1400	0	0	0
20	245	1800	1400	1400	0	0	0
20	250	1900	1600	1600	300	0	0
20	255	2100	2000	2000	1000	0	0
20	260	2200	2100	2100	1100	0	0
20	265	2200	2100	2100	1200	0	0
20	275	1900	1900	1900	1200	300	0
20	280	1600	1800	1800	1900	1400	0
20	285	1200	1100	1100	900	800	800
20	290	600	800	800	700	400	10
20	305	400	400	0	0	0	0
20	310	2000	2000	800	800	1000	200
20	315	2600	2600	2700	2650	2500	2600
20	320	3200	3150	3100	3050	3000	3000
20	325	3500	3450	3300	3200	3100	3050
20	330	2000	1950	1900	1600	1200	800
20	335	200	100	0	0	0	0
25	230	1000	500	300	0	0	0
25	235	1200	1550	1500	0	0	0
25	240	1800	1850	1800	0	0	0
25	245	2100	2000	2000	50	0	0
25	250	2300	2500	2400	1200	0	0
25	255	2600	2800	2800	1800	0	0
25	260	2600	3100	3100	2400	1000	0
25	265	2800	2800	2800	2800	1000	500
25	270	3000	2700	2700	2400	1000	0
25	275	2800	2700	2650	2000	600	0
25	280	2500	2350	2200	2400	1000	0
25	285	1950	2050	2050	1800	1200	0
25	290	1000	1500	1500	1100	1000	500

Appendix 1 (*continued*)

Colat	E-Long	18	14	12	10	8	6
25	310	1800	1800	1000	1000	1000	500
25	315	2700	2700	2650	2650	2600	2600
30	225	1000	900	0	0	0	0
30	230	1000	900	800	0	0	0
30	235	1000	900	0	0	0	0
30	240	1200	1400	1300	0	0	0
30	245	2000	1850	1800	0	0	0
30	250	2400	2200	2000	0	0	0
30	255	2500	2400	2300	1100	400	0
30	260	2800	3050	2600	2100	1500	0
30	265	3200	3400	2900	2100	1200	0
30	270	3500	3400	3000	2050	600	0
30	275	3400	2800	2500	1800	400	0
30	280	3100	2400	2400	1600	400	0
30	285	2600	2050	2100	1400	600	0
30	290	1800	1500	1600	1300	600	0
30	295	500	800	600	700	300	0
30	315	200	100	0	0	0	0
35	230	1500	1400	1000	500	0	0
35	235	1500	1400	1000	0	0	0
35	240	1000	1000	0	0	0	0
35	245	1600	1000	200	0	0	0
35	250	2000	1800	1000	0	0	0
35	255	2000	2200	1100	0	0	0
35	260	2000	2400	1400	800	200	0
35	265	2400	2800	1900	1600	1200	0
35	270	2800	3050	2200	2000	900	0
35	275	3000	3400	2800	2100	700	0
35	280	3500	3400	3250	2100	600	0
35	285	3000	3100	3000	2800	800	0
35	290	2000	2200	2500	3000	2000	500
35	295	1400	1400	1750	1600	140	0
35	300	600	600	600	0	0	0
40	235	1500	1300	0	0	0	0
40	240	1500	1000	1000	0	0	0
40	245	1000	800	0	0	0	0
40	250	800	0	0	0	0	0
40	255	900	300	0	0	0	0
40	260	1400	1200	0	0	0	0
40	265	1800	1900	0	0	0	0
40	270	2000	2200	900	300	0	0
40	275	2400	2700	1600	900	0	0
40	280	2800	2850	1850	1300	300	0
40	285	2800	2850	2100	1200	0	0
40	290	2600	2050	900	700	0	0
40	295	1800	1500	0	0	0	0
40	300	1700	1300	0	0	0	0
40	305	0	600	0	0	0	0
45	265	1200	1000	0	0	0	0
45	270	0	200	0	0	0	0
45	275	1900	900	200	0	0	0
45	280	1900	1400	900	0	0	0
45	285	1900	1400	200	0	0	0
45	290	1700	1200	800	0	0	0
45	295	1200	900	0	0	0	0
50	275	300	0	0	0	0	0
50	280	300	0	0	0	0	0
			Fennoscandia Ice				
10	15	900	800	500	200	0	0
10	20	900	800	500	200	0	0

Appendix 1 (*continued*)

Fennoscandia Ice (*continued*)

Colat	E-Long	18	14	12	10	8	6
10	25	900	800	500	200	0	0
10	40	100	800	0	0	0	0
10	45	500	200	200	100	0	0
10	50	500	200	200	100	0	0
10	55	500	200	200	100	0	0
10	60	500	200	200	100	0	0
10	65	100	50	0	0	0	0
15	65	500	400	300	100	0	0
20	20	800	400	0	0	0	0
20	25	1500	1400	800	0	0	0
20	30	1500	1400	0	0	0	0
20	35	500	200	0	0	0	0
20	65	500	400	200	0	0	0
25	340	1500	1200	900	500	0	0
25	345	1000	700	0	0	0	0
25	15	1800	1700	1000	800	0	0
25	20	2900	2750	2250	1800	0	0
25	25	3000	2850	2300	1900	0	0
25	30	2900	2600	2350	500	0	0
25	35	2500	2300	2300	0	0	0
25	40	1500	1200	500	0	0	0
25	45	200	0	0	0	0	0
25	65	100	0	0	0	0	0
30	5	800	200	0	0	0	0
30	10	1500	1300	1000	900	0	0
30	15	2000	1800	1700	700	0	0
30	20	2800	2500	1900	50	0	0
30	25	2800	2600	2000	0	0	0
30	30	2800	2600	500	0	0	0
30	35	1200	50	100	0	0	0
30	40	50	0	0	0	0	0
35	355	2000	1600	500	0	0	0
35	10	500	0	0	0	0	0
35	15	1200	700	0	0	0	0
35	20	1300	900	0	0	0	0
35	25	800	0	0	0	0	0

Appendix 2

Detailed description of sites

Site 1, North-eastern Ellesmere Island—England (1974)

England (1974) collected and dated several samples of marine shells in the bays and fiords of this region. The area is only 50–100 km from the north-west coast of Greenland and thus may be partly affected by the history of the Greenland ice cap as well as by the local ice caps and glaciers of the Innuitian ice cap (or Franklin complex?, *cf.* England 1974). The uncorrected field observations (i.e. no eustatic sea-level correction) lie above the predicted values although roughly parallel. The ' edge ' effect is seen in the first two thousand years after deglaciation but the curves do not flatten as rapidly at other edge sites (e.g. sites 6 and 10). The dated sites suggest that the ice unloading history is not accurately specified. Agreement could be improved by delaying deglaciation in this region. It is possible that we are also seeing some effect of the $5 \times 5°$ grid on the detailed unloading history of a site not near the grid point.

Site 2, Melville Island—Henoch (1964)

This site lies at the extreme north-western margin of the Laurentide ice sheet. Since the curve was published in 1964, more dates have become available but do not alter the gross form of the rebound. Again the field data are plotted at uncorrected elevations. Model 1 and the field data are roughly parallel but offset by about 2500 years. This might be partly explained by the method of removing the ice in steps as opposed to a continuous slow retreat. There is no evidence for the sinking observed in Model 1 after 9000 BP although sea level was close to present for at least the last 2000 years. The present rate of uplift is minimal and certainly lower than suggested by Model 3.

Site 3, Eastern Baffin Island—Løken (1965)

This site is located very close to the margin of the north-eastern sector of the Laurentide ice sheet. At the most ice extended 20–50 km beyond this site. The main point of interest is thus why is the fit between Model 1 and the field data so good? Why is there no dramatic edge effect as shown for example in site 6? The field data are uncorrected but since the sea-level correction would be addition this makes numerical agreement nearly perfect.

Site 4, Ottawa Islands, Hudson Bay—Andrews & Falconer (1969)

The Ottawa Islands lie close to the central ridge of the former Laurentide ice sheet. The agreement between Model 1 and the field observations is excellent, whereas Model 3 shows a form that is quite unacceptable, with a predicted present rate of uplift far in excess of that demanded by the C^{14} dated samples. The ice-unloading history that was used over Hudson Bay has been previously discussed by Andrews & Peltier (submitted).

Site 5, Vancouver, BC—Matthews et al. (1970)

This site lies close to the south-western margin of the Cordilleran ice sheet. The ice-unloading history appears reasonable in as much as the magnitude of the rebound is closely predicted. However, recovery along the outer coast of BC was nearly instantaneous, and this is not shown by either model. Presumably this site shows the fast relaxation typical of sites close to the edge with the rebound strongly influenced by the flexing of the lithosphere.

There is some data to suggest that a relatively minor re-advance (the Sumas) caused a reversal and led to renewed submergence. This effect could not be examined in our study because of the lack of temporal resolution. It would be interesting to examine whether such a significant reversal of rebound could be modelled—if it could not, then other explanations could be sought.

Site 6, St Lawrence Lowlands—Elson (1969)

The St Lawrence Lowlands lay within about 400 km of the margin of the Laurentide ice sheet, but the ice thickness estimates are complicated by the presence of mountains between the Lowlands and the ice margin and also by the possibility that during glaciation there were distinct glacial centres along the south-eastern margin of the ice sheet. This was certainly the case in the Maritimes of Canada (Grant 1975). The St Lawrence glacio-isostatic adjustment shows reasonable accord with the field evidence (Elson 1969) particularly the flattening of the rebound close to 8000 BP. However, the field data suggest that the initial recovery was more rapid than predicted under Model 1 which suggest a slight but significant effect introduced by the lithosphere. The field curve lies well to the left of the predicted curve suggesting that the unloading was delayed more than we have assumed in our ice-history model.

The curves could be reconciled by postulating a stable ice cover that very rapidly disintegrated about 12 500 BP as the Champlain Sea flooded into the Lowlands.

Site 7, coastal Maine—Stuiver & Borns (1975)

The coast of Maine is located close to the margin of the Laurentide ice sheet during the late Wisconsin glacial maximum. The field evidence indicates conclusively that rebound was extremely rapid with deglaciation occurring about 13 000 BP and with present sea level crossed only a few hundred years later. Observed emergence is about 120 m at sites a few tens of kilometres from the coast and thus with a sea-level correction the observed and predicted recovery would be close, indicating that the unloading history is not unreasonable. However, the observed rebound is similar in form to that at Vancouver (site 5) and indicates the dominating imprint of the recovery of the elastic lithosphere. It is strange, however, that the rate of recovery near present is still quite considerable under the model whereas a curve as in site 6 would be similar to the field evidence. Note that the same statement can be made about the recovery at site 5.

Site 8, New Jersey—Stuiver & Daddario (1963)

New Jersey lies 100 km or so beyond the margin of the Laurentide ice sheet's most extensive late Wisconsin advance. The relative sea-level curve for Brigantine, NJ (Stuiver & Daddario, 1963) shows a 13-m submergence over the last 7500 yr. In contrast the glacio-isostatic rebound models indicate uplift of about 9–14 m over the same interval of time. A sea-level correction of close to 10 m at 7000 BP is a feature of many eustatic sea-level curves and this added to the relative sea-level curve indicates that there has been possibly 3 m or so of submergence. The site may lie in an area affected by the migration and/or collapse of the forebulge (??).

Site 9, Florida—Scholl et al. (1969)

The Florida site lies 20° latitude south of the Laurentide ice margin. The uniform viscosity model and the model including ocean filling run parallel to each other and are only separated by 4 m at most. The observed C^{14} dated submergence curve (Scholl *et al.* 1969) fits perfectly onto either model and contrasts with the results predicted by the high viscosity lower mantle model which would indicate the slight uplift taking place today. The results of this comparison may suggest that in the 7000 years there has been very little eustatic sea-level rise—this is an important result. Further verification of the model would have to come from shallow cores penetrating back in time to 15 000 BP. Taken together sites 4 and 9 are strong evidence that the viscosity of the lower mantle cannot be significantly in excess of that in the upper mantle.

Site 10, West Greenland—Ten Brink (1974); Kelly (1973)

The sites from West Greenland lie close to the present margin of the Greenland ice cap which has remained relatively stable over the last 6000 years. The position of the ice edge during the late Wisconsin maximum is not known with any certainty and nearly all published C^{14} dates are 9000 years old or less. Kelly's data came from an area about 100 km from the present ice edge. The observed data show a rapid nearly instantaneous recovery with values close to 100–140 m in 8000–9000 yr. The position of sea level after 5000 BP is not well documented, but the consensus appears to be that it was close to present. A slight submergence has been reported at sites around the Greenland coast. The observed rebound occurs much faster than predicted by either model and again appears to show the influence of a rapid relaxation of the lithosphere. The predicted curves lie well to the right of the observed, suggesting that the ice unloading history needs to be adjusted to show a relatively stable ice configuration up to about 10 000 BP and then a rapid thinning and retreat.

Site 11, East Greenland—Washburn & Stuiver (1962); Lasca (1966)

The East Greenland sites lie within 100 km of the present ice margin. Deglaciation occurred at approximately the same time as over the West Greenland site with C^{14} dates close to 9000 years old. The observed recovery is not closely controlled, but nevertheless the very rapid rebound is a fact, and it appears that there has been relatively little recovery in the last 5000 years. The observed data lie well to the left of the predicted curves and the same explanation can be advanced as for site 10, i.e. that the Greenland ice cap was stable until about 10 000 BP and then rapid retreat occurred. In the East Greenland case the predicted amount of deflection is 55–80 m, and this is too low in view of the 70+20 = 90 m of postglacial uplift. This could be a problem in the actual ice load or else it might reflect the problem of a 5° grid (ice sheets are strongly parabolic in profile within the first 200 km from the ice margin).

Site 12, North-west England—Tooley (1974); Andrews et al. (1973)

The southern margin of the Lake District was glaciated by ice from a local centre, plus ice moving into the Irish Sea Basin from Scotland. During the late Wisconsin maximum, the ice margin is supposed to have lain 100–200 km south of the site. However, the amount of rebound predicted from both models is nearly an order of magnitude greater than that observed. Two hundred metres of ice was placed at lat. 55° N and 5° W.

Site 13, Oslo Fiord—Hafsten (1960); Feyling-Hanssen (1963); Kenney (1964)

Oslo Fiord lies at the south-western end of an elongated ridge of present high uplift rates and of high postglacial beaches. It is an analogous position to the southern end of James Bay and Hudson Bay. Present uplift is of the order of 0·8 m/100 yr. The predicted uplift conforms nearly exactly to the observed dated shorelines from about 8000 to the present, but the uplift is much faster and there is more of it in the preceding 1800 yr. The uncorrected marine limit is nearly 220 m asl, and an additional 20–30 m should be added for world sea-level rise over the last 9800 years. We expect that the difference between observation and theory is partly a function of the rapid recovery of the elastic lithosphere and partly reflects the need to delay slightly the load removal.

Site 14, Southern Sweden—Mörner (1969)

The area of South Sweden lies closer to the ice margin than did Oslo Fiord. We chose our site to coincide with the −30-km sea-level curve of Mörner (1969, Fig. 143). This is an excellent site for illustrating anew the large difference between observed and predicted uplift using the high viscosity lower mantle model. In contrast the agreement between the uniform mantle model and dated relative sea levels is substantial. The relative sea-level fall of 65 m in the last 11 200 yr has to be corrected for eustatic sea-level changes (possibly +40) and hence the actual rebound might differ by 50 m from that predicted! This is a large figure, but it can be easily accommodated by a relatively slight shift in the ice withdrawal history—a shift of about 1000 yr would bring the curves into substantial agreement. Part of this problem might, of course, be related to the step nature of the ice unloading at 20000-yr increments.

Site 15, Kong Karls Land—Schytt et al. (1968)

Sites 15, 16 and 17 come from islands that lie on the broad Continental Shelf that fringes the northern European and Russian arctic. The Barents Sea now covers this area, but it is extremely shallow. Schytt *et al.* (1968) suggest, on the basis of the glacio-isostatic rebound, that the area was once covered by a large ice sheet, called the Barents Sea ice sheet. However, the actual age of the ice sheet is not known with certainty and some have suggested that it developed primarily in the early Wisconsin.

In our ice-load model we chose to compute our loads (see Appendix 1) as if there were *no* large Barents Sea Ice Sheet but that there were smaller ice massed located over the islands. We expect then that if our ice-loading model was incorrect we would be *underestimating* the amount of deflection. At site 15 the opposite is the case (see Fig. 15), and even allowing for eustatic sea level, the observed rebound of 70 m is about 50 m less than predicted. On the basis of this one site we would suggest that there is little evidence in the postglacial uplift that supports a major ice sheet centred over the Barents Sea.

Site 16, Hopen—Schytt et al. (1968)

Hopen is a small island located south-east of Spitzbergen. It would thus lie central to an ice sheet centred over the Barents Sea but would be peripheral to an ice load located primarily over the main islands of Spitzbergen. The observed and the predicted rebound are rather similar although the rebound is underpredicted by about 20 m+ whatever sea-level correction we apply. However, the trend of the curves is extremely similar, and we do not see any edge effect.

Site 17, Franz Joseph Land—Grosswald (1972)

Franz Joseph Land would have formed the NE margin of an ice sheet centred over the Barents Sea. The observed relative sea-level history indicates appreciably more rebound than we have predicted using our ice-load history. In addition, there is further suggestion in the rebound curve of the strong relaxation due to the flexing of the lithosphere.

In conclusion, sites 15, 16 and 17 display a variety of agreements between the relative sea level histories and predicted recovery. Overall there appears to be no firm support for a major ice sheet centred over the Barents Sea in late glacial time, but our load histories do require some changes. This region offers a major challenge to the ' inverse problem ' for refinement of the load history as discussed in Paper II.

Site 18, East Caroline Islands—Bloom (1970)

These islands lie a considerable distance from any ice load (Fig. 11). Bloom's radiocarbon dated sea level curve is similar to that from site 9 (Florida) and shows a relative rise of sea level of about 7 m in the last 7000 yr. In the same period of time, the glacio-isostatic change over the islands has amounted to an uplift of *c.* 1·5 m.

Site 19, South Island, New Zealand—Schofield (1964)

Although the South Island of New Zealand supported a small ice complex, it probably had little glacio-isostatic impact at the site which lies close to Christchurch. The rebound at New Zealand is virtually zero over the last 8000 BP, whereas peat found at -18 m is dated at 8000 ± 150 and peat $-0{\cdot}75$ m is dated at 5270 ± 80 BP. These values are close to eustatic sea-level estimates from other sites and indicates no significant tectonic activity at the site, at least over the last 8000 years. We expect that both sites 18 and 19 will be strongly affected by the simultaneous filling of the ocean basins.